Journal of Sound and Vibration 327 (2009) 70–91

Contents lists available at ScienceDirect

Journal of Sound and Vibration

journal homepage: www.elsevier.com/locate/jsvi

Influence of tunnel and soil parameters on vibrations from underground railways

S. Gupta, Y. Stanus, G. Lombaert, G. Degrande *

Department of Civil Engineering, K.U. Leuven, Kasteelpark Arenberg 40, B-3001 Leuven, Belgium

ARTICLE INFO

Article history:
Received 20 November 2008
Received in revised form
19 May 2009
Accepted 23 May 2009
Handling Editor: A.V. Metrikine
Available online 24 June 2009

ABSTRACT

A parametric study is performed to identify the key parameters which have an important influence on the generation and propagation of vibrations from underground railways. In this paper, the parameters related to the tunnel and the soil are considered and their influence on the free field response is studied.

The coupled periodic finite element-boundary element model and the pipe-in-pipe model have been used for this study. Both models account for the dynamic interaction between the train, the track, the tunnel and the soil. A general analytical formulation is used to compute the response of three-dimensional invariant or periodic media that are excited by moving loads. The response to moving loads is written in terms of the axle loads and the transfer functions.

The parametric study can be carried out by separately analyzing the variations in the axle loads and the transfer functions. The axle loads are mainly influenced by the parameters related to the vehicle and the track, while the transfer functions are influenced by the properties of the track, the tunnel and the soil. In the present paper, the parameters related to the tunnel and soil are investigated.

It is observed that the material damping and the shear modulus of the soil have an important influence on the propagation of vibrations. The influence of structural changes to the tunnel as well as geometrical properties such as the size and shape of the tunnel is investigated. It is observed that a larger tunnel results in a smaller response above the tunnel as more energy is radiated downwards. Moreover, it is demonstrated that the tunnel geometry has a considerable influence on the response closer to the tunnel.

1. Introduction

Ground-borne vibration from underground railways is an environmental issue of growing concern. The main origin of the vibration is the dynamic interaction between the train wheels and the rails, resulting in dynamic axle loads that are transferred through the track and the tunnel into the soil. Waves propagate in the soil and impinge on the foundations of nearby buildings, resulting in structural vibrations and re-radiated noise. Ground-borne vibrations in buildings may result into discomfort of people due to mechanical vibration of the human body at frequencies between 1 and 80 Hz or re-radiated noise emitted by vibrating parts of the building at higher frequencies between 16 and 250 Hz [1]. Railway induced vibration may also cause malfunctioning of vibration sensitive equipment.

* Corresponding author.
E-mail address: geert.degrande@bwk.kuleuven.be (G. Degrande).

0022-460X/$ - see front matter © 2009 Elsevier Ltd. All rights reserved.
doi:10.1016/j.jsv.2009.05.029

For design purposes, an evaluation of ground-borne noise and vibration is necessary to assess the environmental impact of railway traffic. Numerical models with varying degree of sophistication have been developed for this purpose. As far as deterministic modeling is concerned, analytical and various numerical methods such as the finite element method [2,3], the boundary element method [4] and integral transform methods have been employed to model the coupled tunnel–soil system. Recently developed models such as the semi-analytical pipe-in-pipe model [5–7], a model based on coupling of the integral transform method and the finite element method [8] and coupled finite element-boundary element models [9–12] account for three-dimensional dynamic interaction between the track, the tunnel and the soil. These advanced models assume the geometry to be invariant or periodic in the longitudinal direction and use the Fourier or the Floquet transform to efficiently formulate the problem in the frequency-wavenumber domain. Researchers have also used alternative methods to model the soil around the tunnel. A 2.5D finite/infinite element approach to model ground-borne vibrations has been proposed by Yang et al. [13,14]. Bian et al. [15] use a 2.5D finite element method with absorbing boundary conditions to model wave propagation from subway traffic.

The pipe-in-pipe model and the coupled periodic finite element-boundary element model have been used to perform a parametric study to identify the key parameters which have an important influence on the generation and propagation of vibrations from underground railways. The mathematical correctness of both models has been demonstrated by validating the methods against each other [16]. The coupled finite element-boundary element model has also been validated by means of several experiments that have been performed in the Cité Universitaire on the line RER B of RATP in Paris and at a site in Regent's Park on the Bakerloo line of London Underground [17]. Despite the large amount of uncertainties present in the problem, a reasonably good agreement has been obtained between the predictions and the measurements.

The objective of the present paper is to study the influence of key parameters on the generation and propagation of vibrations from underground railways. A parametric study is performed on the free field response, which is a function of the soil, the tunnel, the track and the train parameters. As a large number of parameters is involved, some key parameters related to the soil and the tunnel are considered in this paper. Yang et al. [18] have recently performed a parametric study, which is complimentary to the present research. Some findings of that paper are corroborated.

The parametric study is performed by computing the response to a moving train. Random excitation due to rail unevenness and impact excitation due to rail joints and wheel flats are important excitation mechanisms responsible for vibrations in the free field. In the present analysis, only the unevenness excitation and the quasi-static excitation are considered. Since the contribution of the quasi-static forces in the free field is negligible, only the dynamic forces due to rail unevenness are vital for prediction of free field vibrations. It may be noted that the variation in the tunnel and the soil properties has negligible influence on the axle loads and, therefore, the analysis of the transfer functions is sufficient to understand the behavior of tunnel and soil parameters. Nevertheless, the response to moving loads is also computed in order to quantify the effect of certain parameters.

The paper is organized in the following manner. In Section 2, the response of invariant and periodic domains subjected to moving loads is recapitulated. In Section 3, the characteristics of the reference case are summarized and the computation of the transfer functions and axle loads is discussed. In Section 4, the effect of the soil properties such as the shear modulus and the material damping ratio is studied. A tunnel embedded in a dry and saturated soil is also investigated and the difference between the response in both cases is explained. In Section 5, the depth of the tunnel as well as the geometric properties of the tunnel is varied and their influence on the free field vibrations is studied. In Section 6, some important conclusions of the study are summarized.

This paper demonstrates the application of advanced numerical models and elucidates the role of important factors for vibrations from underground railways. It also improves the understanding of generation and propagation mechanisms.

2. Response to moving trains

The coupled track–tunnel–soil system is subjected to vertical loads moving along the longitudinal direction y. In the fixed frame of reference, the distribution of n_a vertical axle loads on the coupled track–tunnel–soil system is written as the summation of the product of Dirac functions that determine the time-dependent position $\mathbf{x}_k = \{x_{k0}, y_{k0} + vt, z_{k0}\}^{\mathrm{T}}$ and the time history $g_k(t)$ of the k-th axle load:

$$\rho \mathbf{b}(\mathbf{x}, t) = \sum_{k=1}^{n_a} \delta(x - x_{k0})\delta(y - y_{k0} - vt)\delta(z - z_{k0}) g_k(t) \mathbf{e}_z \tag{1}$$

y_{k0} is the initial position of the k-th axle that moves with the train speed v along the y-axis and $\mathbf{e}_z$ denotes the vertical unit vector. The response of invariant domains subjected moving loads is given as [17,19]

$$\hat{u}_i(y, \omega) = \frac{1}{2\pi} \sum_{k=1}^{n_a} \int_{-\infty}^{\infty} \hat{g}_k(\omega - k_y v) \tilde{h}_{zi}(k_y, \omega) \exp(-\mathrm{i} k_y (y - y_{k0}))\, \mathrm{d}k_y \tag{2}$$

The response of periodic domains subjected to the moving loads is given as [17,20]

$$\hat{u}_i(\tilde{y}+nL,\omega)=\frac{1}{2\pi}\sum_{k=1}^{n_a}\int_{-\infty}^{\infty}\hat{g}_k(\omega-k_y v)\int_{-L/2}^{L/2}\exp(-\mathrm{i}k_y\tilde{y}')\tilde{h}_{zi}(\tilde{\mathbf{x}}',\tilde{\mathbf{x}},\kappa_y,\omega)\,\mathrm{d}\tilde{y}'\exp(-\mathrm{i}k_y(nL-y_{k0}))\,\mathrm{d}k_y \tag{3}$$

where $\kappa_y=k_y-2m\pi/L$ such that $\kappa_y\in]-\pi/L,\pi/L[$. $\tilde{h}_{zi}(\tilde{\mathbf{x}}',\tilde{\mathbf{x}},\kappa_y,\omega)$ is the transfer function of the coupled track–tunnel–soil system in the frequency-wavenumber domain and is defined as the displacement at $\tilde{\mathbf{x}}$ in the $\mathbf{e}_i$ direction due to a unit load applied at $\tilde{\mathbf{x}}'$ in the $\mathbf{e}_z$ direction. Expression (3) shows that the response to moving loads can be calculated from the transfer functions and the axle loads.

The transfer functions $\tilde{h}_{zi}(k_y,\omega)$ in case of invariant domains are calculated using the semi-analytical pipe-in-pipe model [5–7], while the transfer functions $\tilde{h}_{zi}(\tilde{y}',\tilde{y},\kappa_y,\omega)$ in case of periodic domains are computed using the coupled periodic finite element-boundary element model [9,10]. In the following, the lateral $\hat{h}_{zx}(y',y,\omega)$ and the vertical $\hat{h}_{zz}(y',y,\omega)$ transfer functions of the system are analyzed to study the influence of the tunnel and the soil parameters.

3. Reference case

3.1. System characteristics

An invariant tunnel embedded in a homogeneous half-space at a depth $d_t=20\,\mathrm{m}$ is considered. The tunnel has an internal radius $r_i=2.7\,\mathrm{m}$ and a wall thickness $t=0.3\,\mathrm{m}$. The tunnel has a concrete lining with Young's modulus $E_t=35\,000\,\mathrm{MPa}$, Poisson's ratio $\nu_t=0.25$, a density $\rho_t=2500\,\mathrm{kg/m^3}$ and a hysteretic material damping ratio $\beta_t=0.02$. The homogeneous half-space has a shear wave velocity $C_s=250\,\mathrm{m/s}$, a longitudinal wave velocity $C_p=500\,\mathrm{m/s}$, a density $\rho=1750\,\mathrm{kg/m^3}$ and a hysteretic material damping ratio $\beta=\beta_s=\beta_p=0.025$ in shear and volumetric deformation.

A conventional non-ballasted concrete slab track is considered in the tunnel. The track consists of UIC 60 rails with a mass per unit length $\rho_r A_r=60\,\mathrm{kg/m}$ and a bending stiffness $E_rI_r=6.4\times10^6\,\mathrm{N\,m^2}$. The rails are discretely supported on soft rail pads at an interval of 0.6 m. The vertical stiffness of the rail pads is $k_{\mathrm{rp}}=50\,\mathrm{MN/m}$. These rail pads are commonly present on directly fastened tracks. The rail pads rest on a concrete slab that has a mass per unit length $m_{\mathrm{sl}}=2450\,\mathrm{kg/m}$ and a bending stiffness $E_{\mathrm{sl}}I_{\mathrm{sl}}=433\times10^6\,\mathrm{N\,m^2}$. The slab is rigidly connected to the tunnel invert. As the pipe-in-pipe model can only model a circular tunnel lining and cannot consider a tunnel invert, the tunnel invert is disregarded in the parametric study and the slab is directly connected to the tunnel lining. The track is modeled as a double beam on an elastic foundation (Fig. 1). The upper beam represents the two rails, while the lower beam represents the slab. The rail pads are modeled as a continuous support between both beams, while the connection between the slab and the lining is modeled as a continuous support below the lower beam. Since a homogeneous track model is used, the stiffness of the rail pads is smeared in the longitudinal direction. Thus, the stiffness of the continuous support representing the rail pads is $\bar{k}_{\mathrm{rp}}=2k_{\mathrm{rp}}/d=166.6\,\mathrm{MN/m^2}$. The damping in the rail pads is often difficult to estimate and should be determined from rail receptance tests. The hysteretic damping in the rail pads is represented by a complex stiffness $K_{\mathrm{rp}}=\bar{k}_{\mathrm{rp}}(1+\mathrm{i}\eta_{\mathrm{rp}})$. In the present case, a loss factor of $\eta_{\mathrm{rp}}=0.3$ is assumed in the rail pads.

The rail unevenness $u_{w/r}(y)$ is expressed as a stochastic process characterized by a single-sided power spectral density (PSD). For the present study, FRA track class 6 is used, which corresponds to the best quality rail according to FRA standards [17,21,22].

The train consists of six cars each of length 19 m. The bogie and axle distances on all cars are 12.6 and 2.3 m, respectively. The total mass of the train is 342 tons, resulting in an axle load of 139.8 kN. The mass of the coach with passengers is 43 tons, while the mass of the bogie and axle is 3.6 and 1.7 tons, respectively. The primary suspension has a stiffness $K_1=1.4\times10^6\,\mathrm{N/m}$ and a damping $C_1=3\times10^4\,\mathrm{N\,s/m}$. The secondary suspension has a stiffness $K_2=5.8\times10^5\,\mathrm{N/m}$ and a damping $C_2=1.6\times10^5\,\mathrm{N\,s/m}$. The speed of the train is considered to be $v=60\,\mathrm{km/h}$.

3.2. Transfer functions

The track–tunnel–soil system can be modeled using the pipe-in-pipe [5,6,23] model or the coupled periodic finite element-boundary element model [9,10,17].

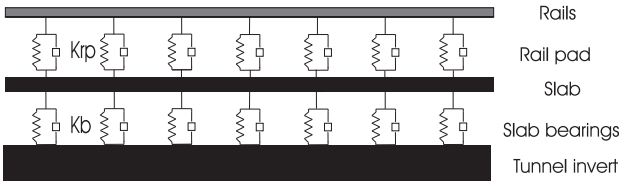

Fig. 1. Track model for the rails supported on a slab.

The pipe-in-pipe model assumes the geometry in the longitudinal direction to be invariant and uses the Fourier transform to formulate the problem in the frequency-wavenumber domain. The load on the tunnel lining is decomposed using Fourier series [5,7]. The shell equations for the tunnel and the wave equations for an elastic continuum representing the soil [5,7] are written in cylindrical coordinates and solved analytically to calculate the displacements for each component. The displacement field is then calculated by summing the displacements calculated for all Fourier series components. For the present analysis, it has been found that 10 terms in the Fourier series are sufficient to obtain convergence [17]. The original pipe-in-pipe model could only be used for circular tunnels embedded in a full space. The pipe-in-pipe model has been extended to account for the free surface as well as multilayered ground [24].

The coupled periodic finite element-boundary element model accounts for the complex periodic geometry of the tunnel as well as the layering of a semi-infinite soil medium. The periodic approach has been previously applied for the seismic analysis of sheet pile walls of infinite length [25–27]. Considerable progress has been made regarding the solution of dynamic soil–structure interaction problems defined on periodic domains, using coupled periodic finite element-boundary element formulations and has been used to model tunnels embedded in a layered half-space [9,10]. The coupled periodic finite element-boundary element model uses the Floquet transform to exploit the periodicity (or invariance) in the longitudinal direction. It is based on a subdomain formulation where a finite element method is used for the track and the tunnel, while a boundary element method is used for the soil.

In the coupled finite element-boundary element approach, the tunnel displacements are decomposed on the basis of functions $\tilde{\Psi}_t(\tilde{\mathbf{x}}, \kappa_y)$, while the soil displacements are written as a superposition of waves that are radiated from the tunnel [9,10]. The kinematical basis is selected by performing an eigenvalue analysis of the tunnel's reference cell [17]. The kinematical basis must obey the periodicity condition of the second kind in order to comply with the definition of the Floquet transform [9,10,17]. A complex eigenvalue problem is formed at each wavenumber after imposing the periodicity condition of the second kind on the reference cell [17]. In the present analysis, the eigenvalue problem is solved for only a limited number M of lower modes at selected wavenumbers $[\kappa_{y1}, \kappa_{y2}, \ldots, \kappa_{yq}]$ in the range $[0, \pi/L]$. Fig. 2 shows three in-plane flexible modes of the generic cell computed at zero wavenumber. The eigenvectors computed at selected wavenumbers are collected in a matrix and a singular value decomposition is applied to obtain the kinematical basis. In the following, a kinematical basis consisting of 60 vectors has been used for the analysis.

Even though periodicity of the track–tunnel–soil system is exploited, the coupled periodic finite element-boundary element model is still quite demanding from a computational point of view. In the following, the coupled periodic finite element-boundary element model and the pipe-in-pipe model are used to perform a parametric study.

Fig. 3 shows the location of the observation points in the free field with respect to the tunnel. The response is calculated at these reference points in the free field. The coordinates of these observation points are summarized in Table 1.

Fig. 4 shows the vertical transfer function of the coupled tunnel–soil system in the free field at points A, C, D, E, G and H (Fig. 3). Fig. 5 shows the horizontal transfer function of the coupled tunnel–soil system in the free field at points B, C, D, F, G and H (Fig. 3). It should be noted that the horizontal response is shown at a lateral distance of 4 m at the surface (point B) and at depth (point F) instead of the points directly above the tunnel. This is because the horizontal displacement at points directly above the tunnel due to a vertical load on the tunnel invert is zero. The soil around the tunnel allows for the radiation of energy in the radial direction. The transfer functions in the free field are characterized by an undulating behavior, which is due to interference of compression and shear or Rayleigh waves. The frequency step in the interference pattern depends on the distance of the observation point from the source as well as the compression and shear wave velocity in the ground. Superimposed on these graphs are the Green's function of the half-space. Comparison between the Green's functions and the transfer functions gives an insight into the behavior of the coupled tunnel–soil system. At low frequencies, the transfer functions are identical to the Green's functions as the wavelengths in the soil are much larger than the diameter of the tunnel and the response in the free field is strongly influenced by the dynamic characteristics of the soil. At higher frequencies, the wavelengths are comparable to the diameter of the tunnel and the response in the free field

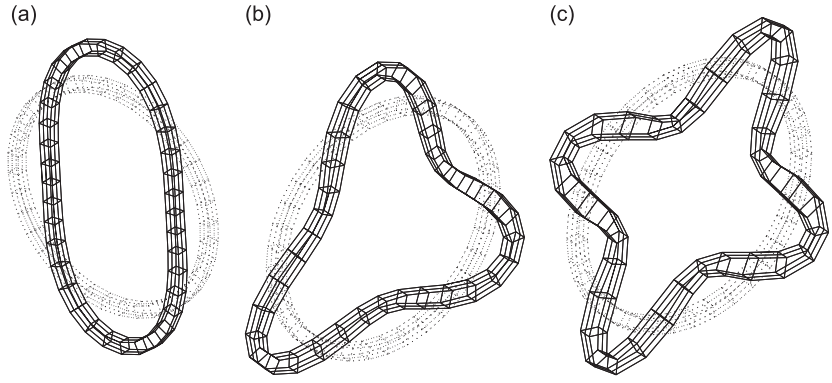

Fig. 2. The in-plane flexible modes at (a) 17.84 Hz, (b) 51 Hz and (c) 99.28 Hz of the reference cell of the tunnel without the concrete invert.

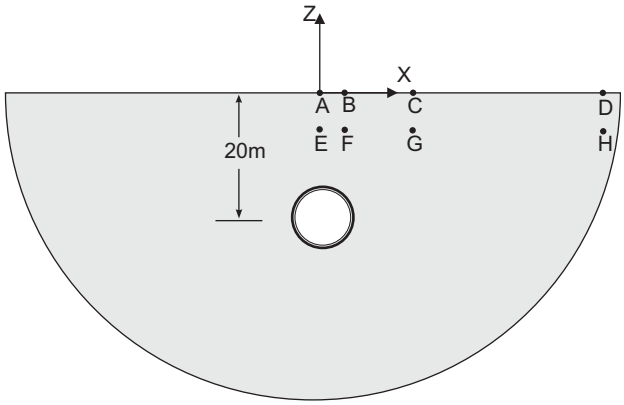

Fig. 3. Location of the observation points in the free field.

Table 1
Coordinates of the observation points.

Points	x (m)	y (m)	z (m)
A	0	0	0
B	4	0	0
C	16	0	0
D	64	0	0
E	0	0	−4
F	4	0	−4
G	16	0	−4
H	64	0	−4

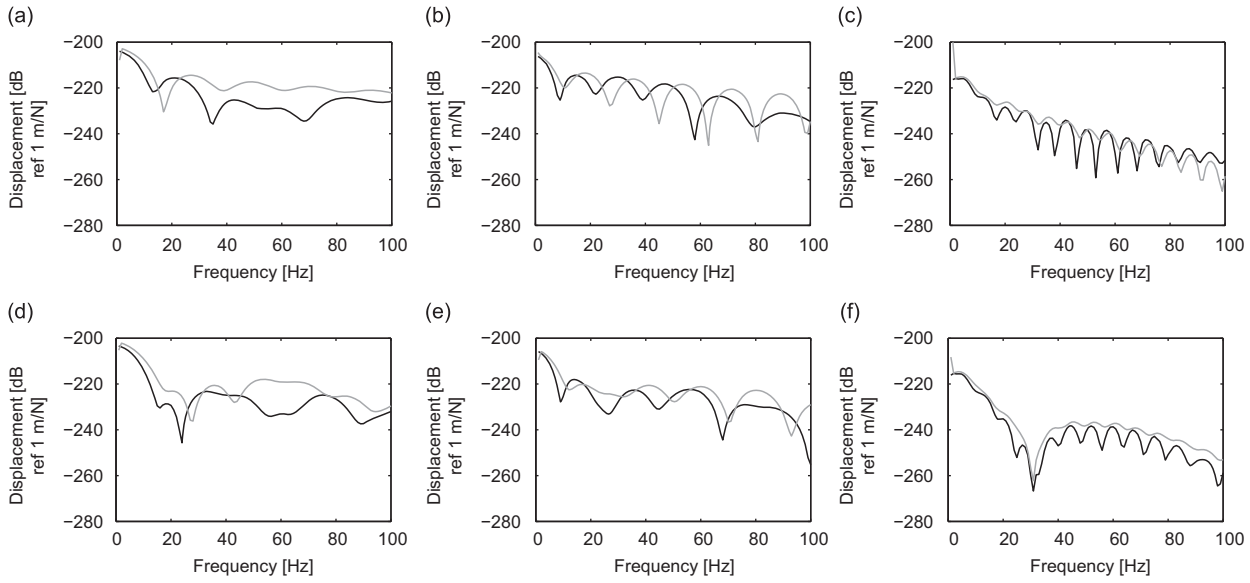

Fig. 4. Vertical transfer function (black line) in the free field at points (a) A, (b) C, (c) D, (d) E, (e) G and (f) H for a tunnel embedded in a half-space. Superimposed on the graphs is the Green's function of a homogeneous half-space (gray line).

largely depends on the dynamic interaction between the tunnel–soil system and, therefore, differs from the Green's functions. The influence of certain parameters such as material damping and the presence of soil layering (far from the tunnel) can be studied using only the Green's function, as they do not significantly modify the tunnel–soil interaction. In the present study, however, the transfer functions of the track–tunnel–soil system are used to investigate the influence of all parameters.

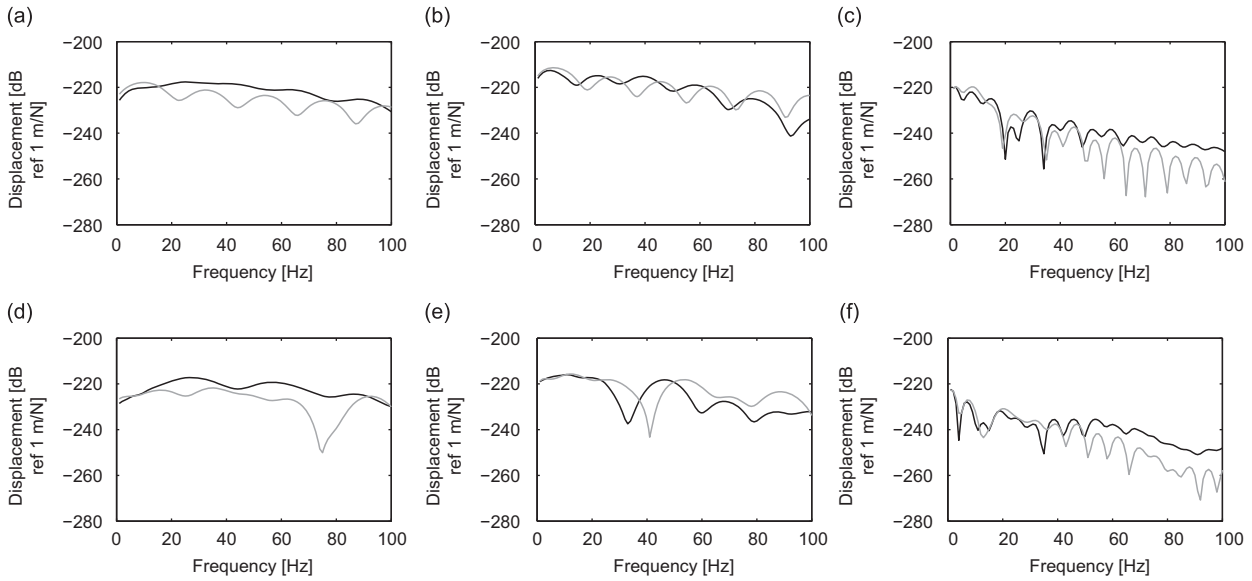

Fig. 5. Horizontal transfer function (black line) in the free field at points (a) B, (b) C, (c) D, (d) F, (e) G and (f) H for a tunnel embedded in a half-space. Superimposed on the graphs is the Green's function of a homogeneous half-space (gray line).

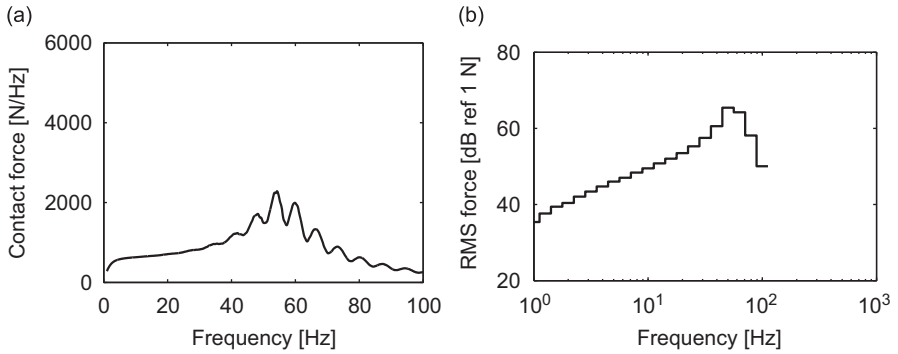

Fig. 6. (a) Frequency content and (b) one-third octave band RMS spectrum of the contact force at the front axle of the train.

3.3. Axle loads

The response in the free field due to a moving train is computed accounting for random excitation due to wheel and rail unevenness. For train speeds lower than the wave velocities in the ground, the quasi-static excitation generates evanescent and leaky waves which decay importantly with distance. Quasi-static excitation has therefore been disregarded in the present analysis of the response in the free field.

The dynamic forces $\hat{\mathbf{g}}_d(\omega)$ due to wheel/rail unevenness can be calculated by considering the vehicle–track interaction as described in Refs. [19,21].

Fig. 6 shows the frequency content and one-third octave band RMS spectrum of the contact force due to wheel–rail interaction for an unevenness profile corresponding to FRA class 6. The effect of the train suspension is only important at low frequencies and has been disregarded in this analysis. The dominant frequency content is around the wheel–track resonance frequency of 58 Hz. It should be mentioned that the axle loads are not significantly affected by the variation in the tunnel and soil parameters. Thus, the influence of the tunnel and soil parameters can be investigated using the transfer functions alone.

4. Variation of the soil parameters

The soil around the tunnel allows the energy to propagate away from the tunnel and get dissipated due to material and geometrical damping in the soil. The amount of energy that propagates through the soil depends on the dynamic interaction between the tunnel and the soil. The response of the tunnel–soil system can be calculated by assembling the dynamic stiffness of the tunnel and the soil. The dynamic stiffness of the soil is a function of the dynamic soil

characteristics such as the shear modulus μ_s, Poisson's ratio v_s, the density ρ and the material damping ratio β. The variation in the soil properties is considered with the aim to perform a sensitivity study rather than a parametric study. The focus is on the variation in the shear modulus μ_s and the material damping ratio $\beta = \beta_s = \beta_p$. The shear modulus and the material damping ratio are determined from a wide range of in situ [28–30] and laboratory tests [28]. The uncertainty associated with the material damping ratio and the shear modulus is usually large. Subsequently, an additional case has been considered to investigate the influence of the tunnel embedded in a dry and a saturated half-space. These studies have been performed using the coupled finite element-boundary element model and verified using the pipe-in-pipe model.

4.1. Soil stiffness

For the reference case, the shear modulus $\mu_s = 109.375$ MPa. A 50 percent variation in the shear modulus is imposed to make the soil stiffer and softer. The change in the shear modulus can be studied using the transfer functions alone, as it is not expected to significantly influence the track compliance and the axle load. This is valid if the stiffness of the track is much smaller than the stiffness of the tunnel–soil system. In the present example, the rails are supported on soft rail pads and the track compliance can also be approximately computed by a track model on a rigid foundation.

The dynamic soil properties for the three cases investigated are summarized in Table 2.

Figs. 7 and 8 compare the vertical and horizontal transfer functions at the surface and at depth for three values of the shear modulus. In the low-frequency range, the modulus of the transfer function decreases with increasing shear modulus due to an increase in the quasi-static stiffness of the soil. At points directly above the tunnel, a similar pattern in the vertical component can be observed in the high frequency range as well. This is because the dynamic stiffness of the soil increases with the shear modulus. The vertical response directly above the tunnel at these high frequencies is influenced by the propagation of compression waves in the vertical direction, while the vertical response further away from the tunnel is more affected by shear waves and Rayleigh waves. The opposite can be said for the horizontal component. To understand this better and to visualize wave propagation in the soil domain around the tunnel, the norm of the displacement vectors for a harmonic excitation at 10 and 80 Hz is displayed in Figs. 9 and 10, respectively. The norm is defined as $|\hat{u}_s| = \sqrt{|\hat{u}_{sx}|^2 + |\hat{u}_{sy}|^2 + |\hat{u}_{sz}|^2}$, where $\hat{u}_{sx}$ and $\hat{u}_{sy}$ are the horizontal transfer functions perpendicular and along the tunnel

Table 2
Different cases for variation in the shear modulus.

Case	Soil type	C_s (m/s)	C_p (m/s)	μ_s ($\times 10^6$ N/m^2)	v_s (–)	ρ (kg/m^3)	β (–)
1	Softer	177	353	54.7	0.333	1750	0.025
2	Reference case	250	500	109.3	0.333	1750	0.025
3	Stiffer	306	612	164.8	0.333	1750	0.025

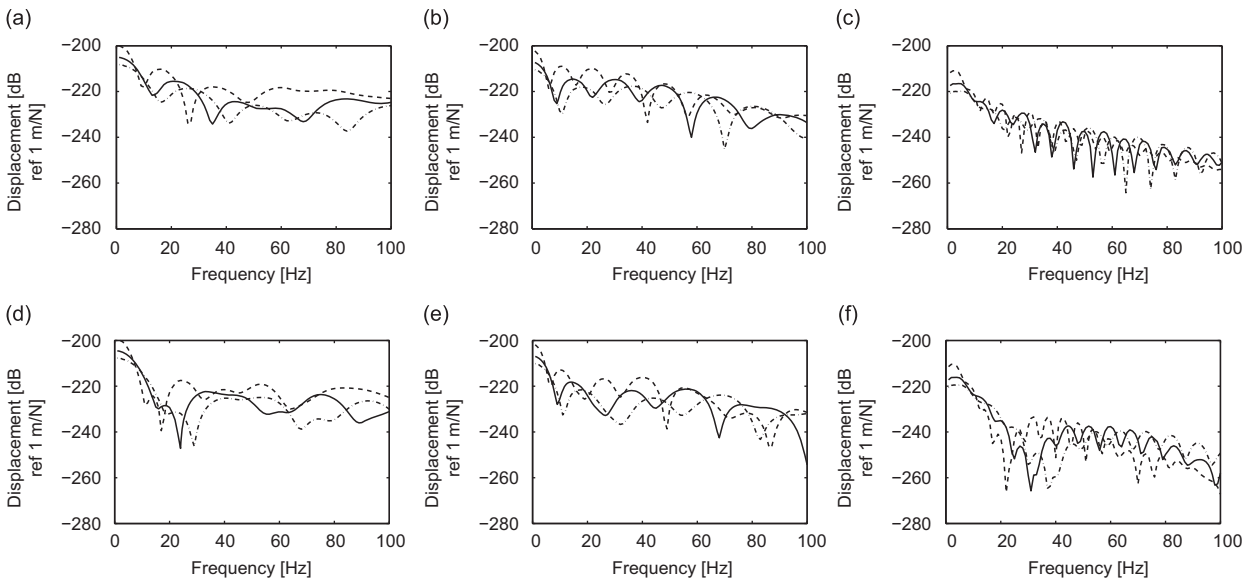

Fig. 7. Vertical transfer function in the free field at points (a) A, (b) C, (c) D, (d) E, (e) G and (f) H for a tunnel embedded in a half-space with shear modulus $\mu_s = 54.68$ MPa (dashed line), $\mu_s = 109.375$ MPa (solid line) and $\mu_s = 164.06$ MPa (dash-dotted line).

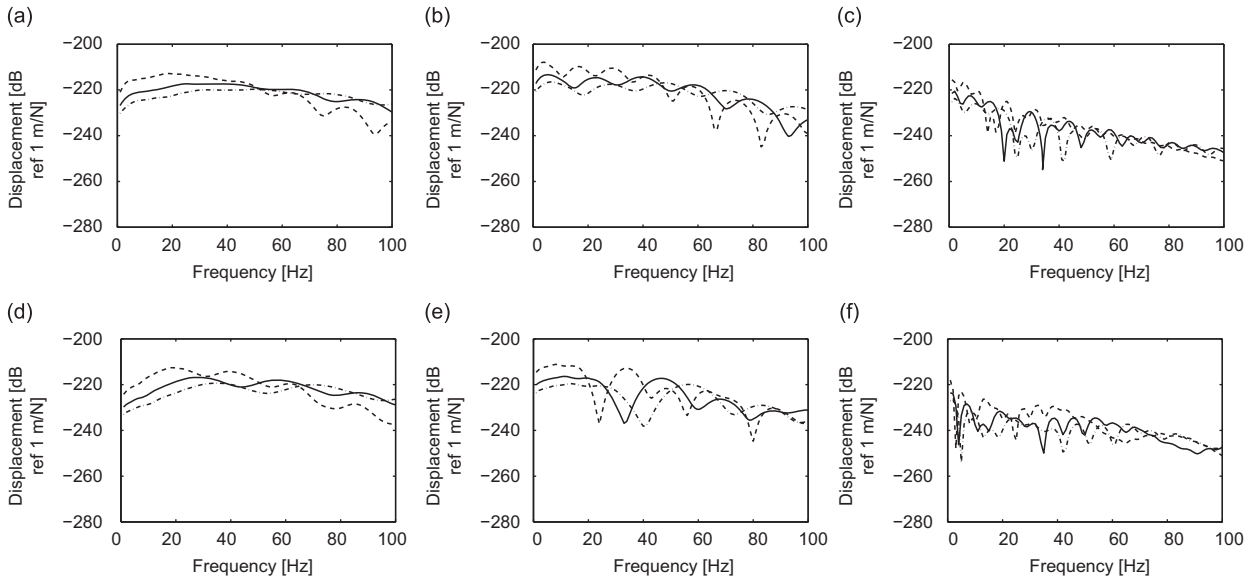

Fig. 8. Horizontal transfer function in the free field at points (a) B, (b) C, (c) D, (d) F, (e) G and (f) H for a tunnel embedded in a half-space with shear modulus $\mu_s = 54.68$ MPa (dashed line), $\mu_s = 109.375$ MPa (solid line) and $\mu_s = 164.06$ MPa (dash-dotted line).

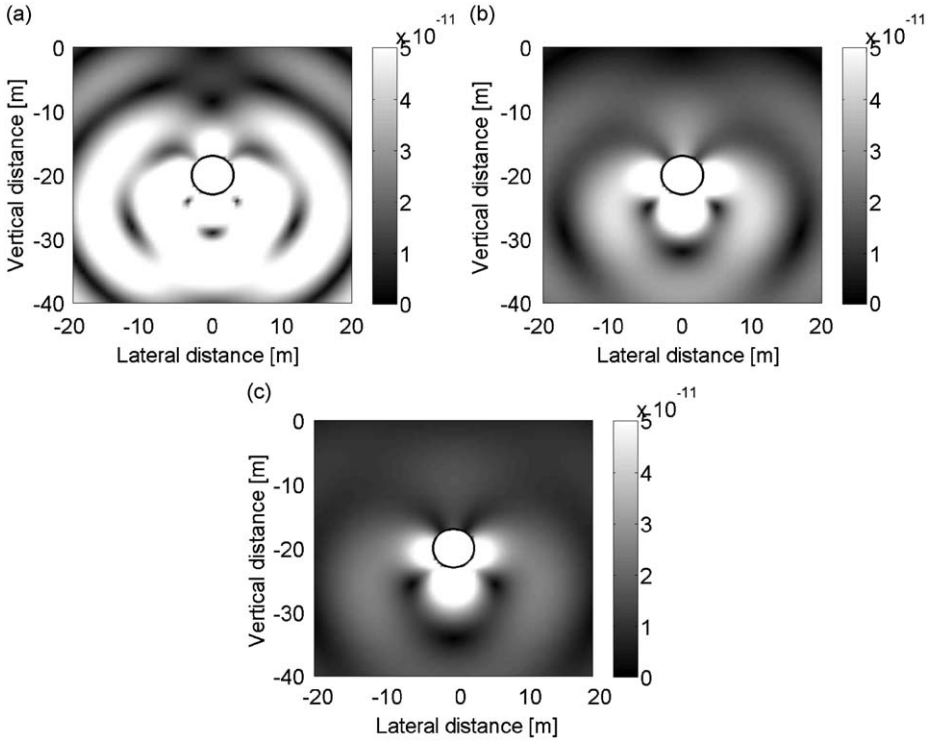

Fig. 9. The norm of the free field displacement vector at a harmonic excitation of 10 Hz for a tunnel embedded in a full space with shear modulus (a) $\mu_s = 54.68$ MPa, (b) $\mu_s = 109.375$ MPa and (c) $\mu_s = 164.06$ MPa.

and $\hat{u}_{sz}$ is the vertical transfer function. It should be noted that since the displacement field is shown in the same plane as the loading, the horizontal component of the displacements $\hat{u}_{sy} = 0$. A similar way of representation has also been used byJones et al. [31] to illustrate the transfer functions. These contour plots are shown for the tunnel embedded in a full space and only give an insight in the wave propagation around the tunnel. The displacements in the soil can be written as a superposition of waves radiated from the tunnel into the soil. The displacements in the vicinity of the tunnel are higher at a low frequency of 10 Hz when the tunnel is embedded in a softer soil (Fig. 9). This results in emission of higher amplitude

waves in the soil. At a higher frequency of 80 Hz, the displacements around the tunnel lining strongly depend on the properties of the tunnel rather than the soil and therefore the displacements in the vicinity of the tunnel are similar for the three cases (Fig. 10). At this frequency, the wavelengths in the soil are shorter than the size of the tunnel and the propagation of vibration is directional such that most of the energy is transmitted downwards. Main interest is, however, in the waves traveling upwards, where foundations of buildings are present. The concentric waves originating at the invert can be seen radiating outwards to the sides of the tunnel and upwards at some lateral distances from the tunnel. These waves are predominantly shear waves.

The pattern of the transfer functions (Fig. 7) is quite complex in the mid-frequency range due to dynamic tunnel–soil interaction. At large distances from the source and at high frequencies, the increase in the vertical response by decreasing the shear modulus is not observed due to the attenuation of the waves in the soil. Whereas the attenuation due to geometrical spreading is independent of the wavelength, the attenuation due to material damping increases as the wavelength decreases. Therefore, the attenuation of waves in a softer soil is greater than in a stiffer soil. In the contour plot for a frequency of 80 Hz (Fig. 10), it can be observed that the vibration levels far from the tunnel are similar in all three cases. This is because the change in dynamic stiffness of the system is compensated by the change in the attenuation of waves at large distances from the tunnel. The effect of material damping in case of a soft soil can also be observed in the horizontal displacement at the free surface closer to the tunnel (Fig. 8a). At large lateral distances, the horizontal response has an important contribution from compression waves as they decay less rapidly with distance. The variation in the shear modulus also causes a phase lag depending on the distance between the source and the receiver and the wavelengths in the soil. At large distances from the tunnel, an undulating behavior in the transfer functions can be explained by interference of the compression and shear or Rayleigh waves. The frequency interval between the troughs in the transfer function is related to the wave speeds in the soil [16] and becomes wider with increasing shear modulus.

For a more detailed assessment of the vibrations from underground railways, the response to a moving load is computed. The axle loads determined in the previous section are used to calculate the response to moving loads by means of Eq. (3). Subsequently, the maximum of the running RMS velocity is calculated, which is extensively used to evaluate human response to vibrations [32]. Fig. 11 shows the maximum RMS of the vertical and horizontal velocity on the free surface as a function of the lateral distance from the tunnel for different cases. Vibration levels are maximum in the case of the softer soil at small distances. At large distances, the maximum RMS of the vertical velocity becomes comparable for all three cases, which is due to a stronger attenuation in the softer soil. It is also interesting to note that, except for the case of the soft soil, the vertical vibration levels are maximum at a horizontal distance of 16 m from the tunnel. This distance depends on the direction of the waves emanating from the tunnel. Above the tunnel a "vibration shadow" in the soil is created where vibration levels are low. The highest levels on the surface usually occur at some lateral distance from the

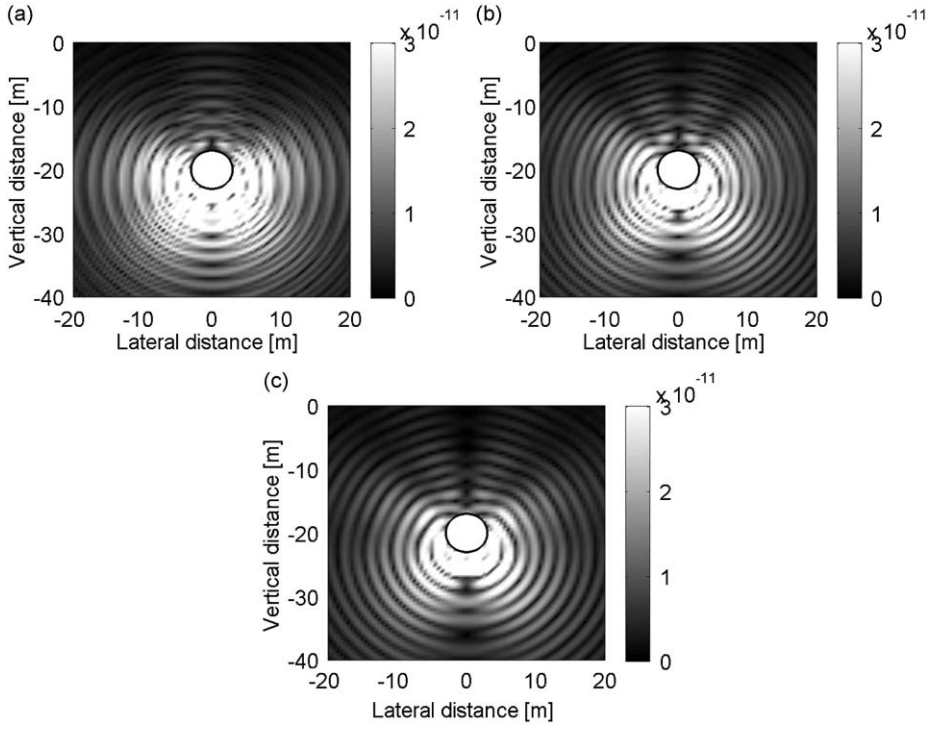

Fig. 10. The norm of the free field displacement vector at a harmonic excitation of 80 Hz for a tunnel embedded in a full space with shear modulus (a) $\mu_s = 54.68$ MPa, (b) $\mu_s = 109.375$ MPa and (c) $\mu_s = 164.06$ MPa.

tunnel. In general, a difference of about 4–6 dB in vertical vibration levels at small lateral distances from the tunnel is observed due to a 50 percent variation in the shear modulus. The influence of this variation in the shear modulus on horizontal vibrations is less compared to its effect on vertical vibrations.

4.2. Material damping ratio

The influence of the material damping ratio is analyzed in the following. The material damping ratio in shear and volumetric deformation is assumed to be the same and is denoted as β herein. Fifty percent variation in the material damping ratio is considered to obtain three cases: $\beta = 0.0125, 0.025, 0.0375$. The effect of the material damping ratio on the dynamic interaction between the tunnel and the soil is not significant and, therefore, it can be studied using the Green's function of a half-space alone. However, the transfer function of the coupled tunnel–soil will be presented in this section.

Figs. 12 and 13 compare the vertical and horizontal transfer functions at the surface and at depth for three values of the material damping ratio. The effect of the material damping ratio is maximum at large distances from the tunnel and higher frequencies. Fifty percent variation in the material damping ratio results in a difference of more than 10 dB in the transfer functions at distances of about 64 m from the tunnel in the higher frequency range. The reduction in magnitude due to material damping depends on the number of vibration cycles the material has undergone. The smaller the wavelength and the larger the distance between the source and the receiver, the larger is the reduction due to material damping. The effect of the material damping ratio on the horizontal and vertical components is similar.

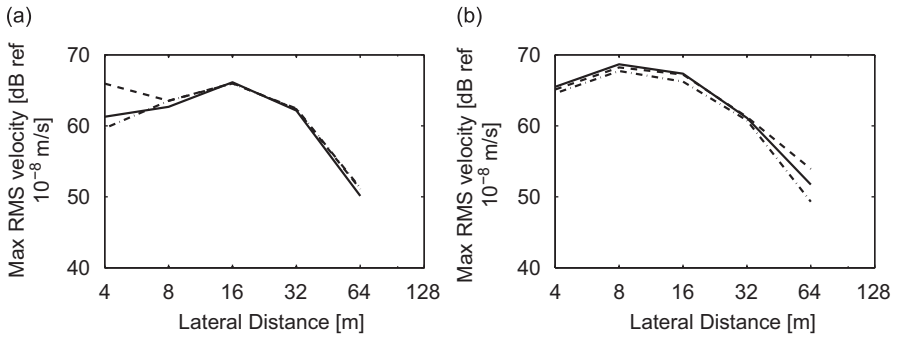

Fig. 11. Maximum RMS of (a) the vertical and (b) the horizontal velocity on the free surface as a function of the lateral distance due to a train running in a tunnel embedded in a half-space with shear modulus $\mu_s = 54.68$ MPa (dashed line), $\mu_s = 109.375$ MPa (solid line) and $\mu_s = 164.06$ MPa (dash-dotted line).

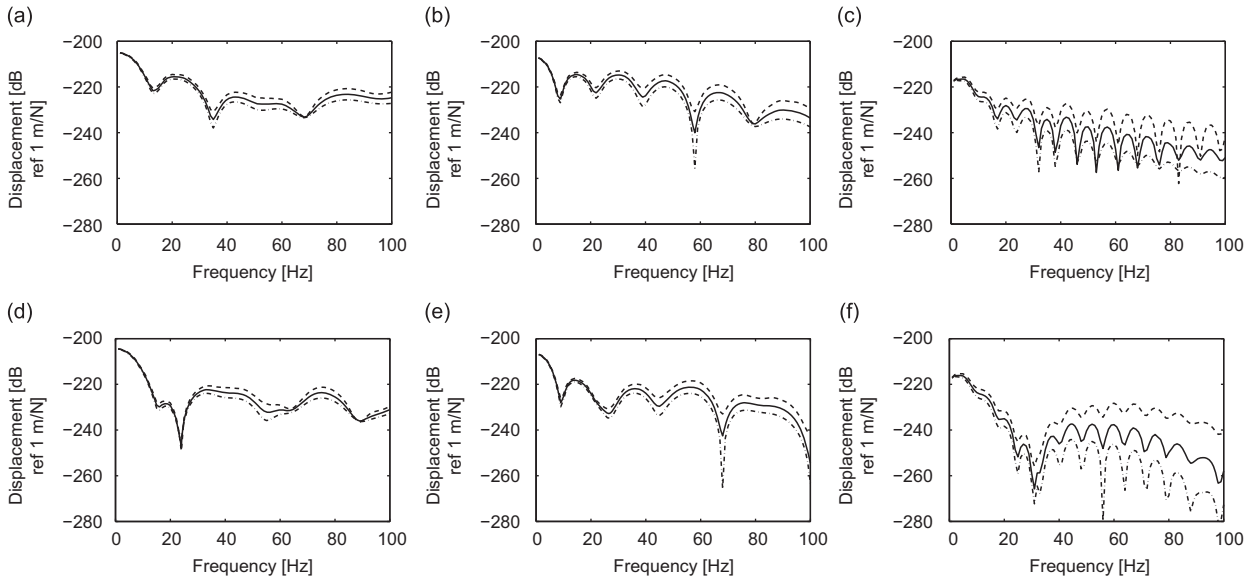

Fig. 12. Vertical transfer function in the free field at points (a) A, (b) C, (c) D, (d) E, (e) G and (f) H for a tunnel embedded in a half-space with material damping ratio $\beta = 0.0125$ (dashed line), $\beta = 0.025$ (solid line), $\beta = 0.0375$ (dash-dotted line).

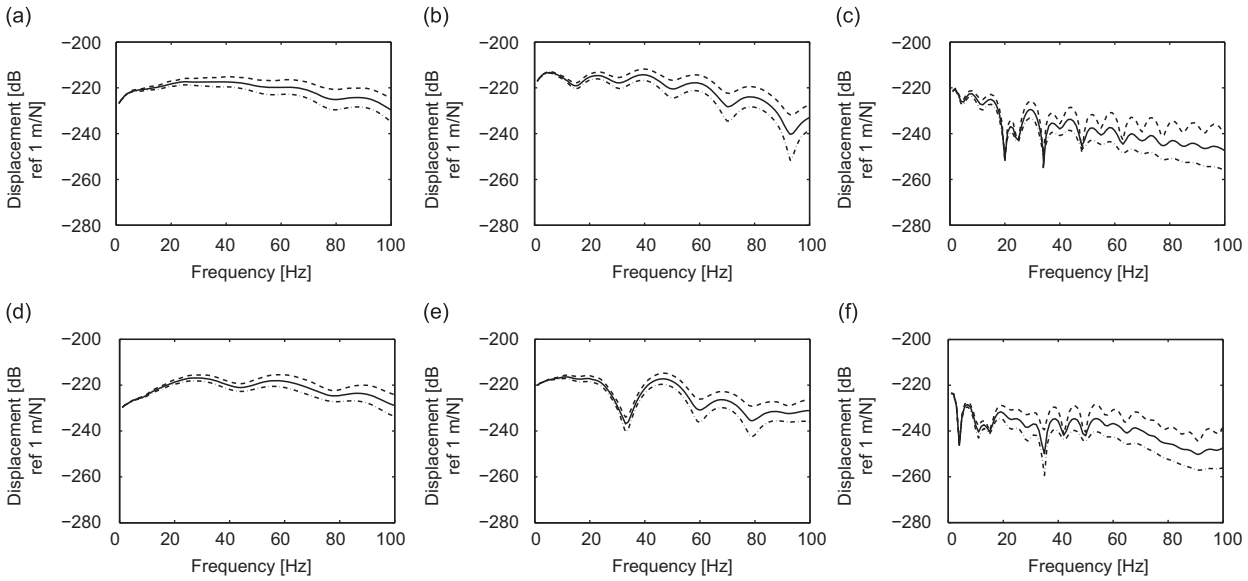

Fig. 13. Horizontal transfer function in the free field at points (a) B, (b) C, (c) D, (d) F, (e) G and (f) H for a tunnel embedded in a half-space with material damping ratio $\beta = 0.0125$ (dashed line), $\beta = 0.025$ (solid line), $\beta = 0.0375$ (dash-dotted line).

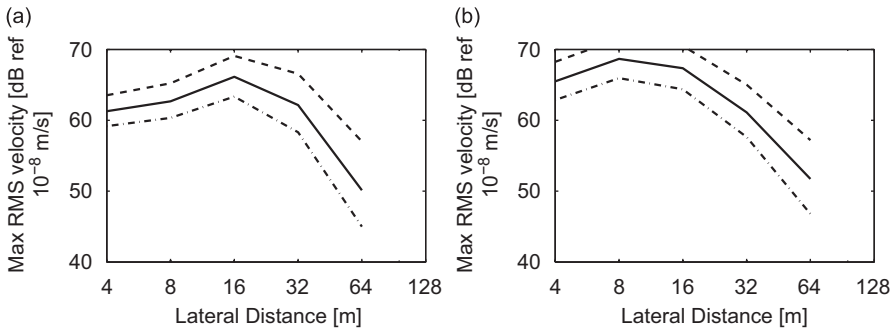

Fig. 14. Maximum RMS of (a) the vertical and (b) the horizontal velocity on the free surface as a function of the lateral distance due to a train running in a tunnel embedded in a half-space with material damping ratio $\beta = 0.0125$ (dashed line), $\beta = 0.025$ (solid line) and $\beta = 0.0375$ (dash-dotted line).

The above calculations are sufficient to show the effect of uncertainty in the material damping ratio. Nevertheless, to better interpret the vibration levels in the free field, the maximum RMS velocity due to a moving train is computed for different values of the material damping ratio.

Fig. 14 shows the maximum RMS velocity as a function of the lateral distance from the tunnel. The difference in the maximum RMS velocity due to a 50 percent variation in the material damping ratio increases with distance from the tunnel. At distances larger than 32 m from the tunnel, a difference of more than 5 dB on the RMS velocity is observed.

4.3. *Dry and fully saturated soil*

A tunnel embedded in a dry soil (reference case) and a fully saturated soil is investigated. The constitutive behavior of soil under dynamic loading is complex. Soil is a discontinuous material, where the pores of the solid skeleton can be (partly) saturated with water. Wave propagation in saturated and unsaturated isotropic poroelastic media can be described by Biot's poroelastic [33,34]. In the low-frequency range of interest in most civil engineering applications, however, a high viscous coupling prevents the relative motion between the fluid and the solid phase and the soil behaves as a frozen mixture. The soil can be modeled as a dry elastic medium, provided that the density and the incompressibility of the saturated soil are accounted for [35]. Thus, the case of a tunnel embedded in a saturated soil is analyzed by considering a higher Poisson's ratio and an equivalent density of the frozen mixture according to Biot's theory. The density of the mixture

ρ is given as

$$\rho = \rho_f n + \rho_s(1-n) \tag{4}$$

where ρ_f is the density of the pore fluid, ρ_s is the density of the solid grains and n is the porosity.

The density of the solid grains consisting of sand is $\rho_s = 2650\,\mathrm{kg/m^3}$, while the density of the dry soil is $1750\,\mathrm{kg/m^3}$. This results in a porosity $n = 0.339$ and the density of the soil–water mixture as $\rho = 2089.6\,\mathrm{kg/m^3}$. The shear wave velocity C_{s0} of the saturated porous medium in the low-frequency limit is equal to

$$C_{s0} = \sqrt{\frac{\mu^s}{\rho}} \tag{5}$$

with μ^s the shear modulus of the dry solid skeleton. The longitudinal wave velocity C_{p0} of the saturated soil in the low-frequency limit can be estimated using the following expression [33]:

$$C_{p0} = \sqrt{\frac{\lambda^s + \mu^s + \lambda^f/n}{\rho_f n + \rho_s(1-n)}} \tag{6}$$

where λ^s and μ^s are the Lamé coefficients of the dry solid skeleton and λ^f is the bulk modulus of the fluid. The Lamé coefficient λ^s can be computed from the shear modulus μ^s and Poisson's ratio ν^s of the dry solid skeleton, which is taken as $\nu^s = \frac{1}{3}$ here. The bulk modulus of the fluid is equal to $\lambda^f = 2.2 \times 10^9\,\mathrm{N/m^2}$. The dynamic soil properties for the dry and saturated soil are summarized in Table 3.

Fig. 15 shows the vertical transfer function in the free field for a tunnel embedded in a dry and a saturated soil. At low frequency, only a small difference between the two cases is observed as the contribution of the shear waves is maximum. The effect of saturation of the medium or the increase in Poisson's ratio can be observed at higher frequencies. The material damping in shear and volumetric deformation is assumed to be the same. Shear waves attenuate more rapidly than

Table 3
Dynamic soil properties of a dry and a fully saturated soil.

Case	Soil type	C_s (m/s)	C_p (m/s)	μ_s ($\times 10^6\,\mathrm{N/m^2}$)	ν_s (–)	ρ ($\mathrm{kg/m^3}$)	β (–)
1	Dry soil (reference case)	250	500	109.3	0.333	1750	0.025
2	Saturated soil	229	1818	109.3	0.492	2089.6	0.025

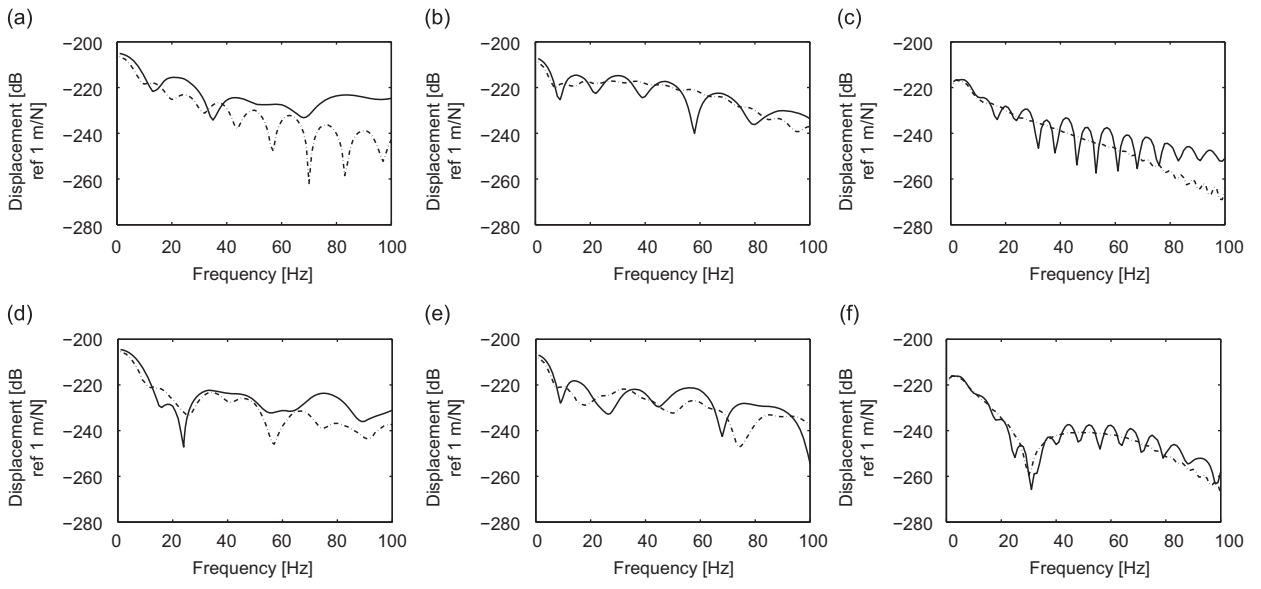

Fig. 15. Vertical transfer function in the free field at points (a) A, (b) C, (c) D, (d) E, (e) G and (f) H for a tunnel embedded in a dry (solid line) and a saturated (dash-dotted line) half-space.

compression waves; in the far field at high frequencies the compression waves are dominant. The contribution of compression waves to the vertical response above the tunnel at higher frequencies is maximum and the difference between the two cases is apparent in Fig. 15a. The vertical response on the free surface above the tunnel in case of the saturated soil is lower than the response of the dry soil due to high compression modulus of the saturated medium. At large lateral distances from the tunnel, the contribution of the compression waves to the vertical displacement is much less and, therefore, the amplitude of the response for the two cases is almost the same (Fig. 15c and f).

Fig. 16 shows the horizontal transfer function in the free field. The points directly above the tunnel are omitted as the horizontal response above the tunnel is zero. The maximum difference between the response for the two cases is seen for points farther away from the tunnel where the contribution of the compression waves is significant (Fig. 16c and f). The horizontal response closer to the tunnel axis is mainly affected by shear waves, and hence is unaffected by the change of Poisson's ratio (Fig. 16a and d).

To visualize the wave propagation in the soil medium, the norm of the instantaneous displacements at 10 and 80 Hz is depicted in Figs. 17 and 18, respectively. In general, it can be observed from the transfer functions that the displacements in the case of a tunnel embedded in a saturated soil are smaller, which can be attributed to the increased dynamic stiffness of the tunnel–soil system.

To quantify the effect of reduction in vibration levels due to saturation of the medium, the response to moving loads is calculated. Fig. 19 shows the maximum RMS of the vertical and horizontal velocity on the free surface as a function of the lateral distance from the tunnel. The effect of Poisson's ratio is maximum on the horizontal component of the free field response far from the tunnel. A difference of more than 10 dB is observed at a lateral distance of 64 m from the tunnel on the free surface.

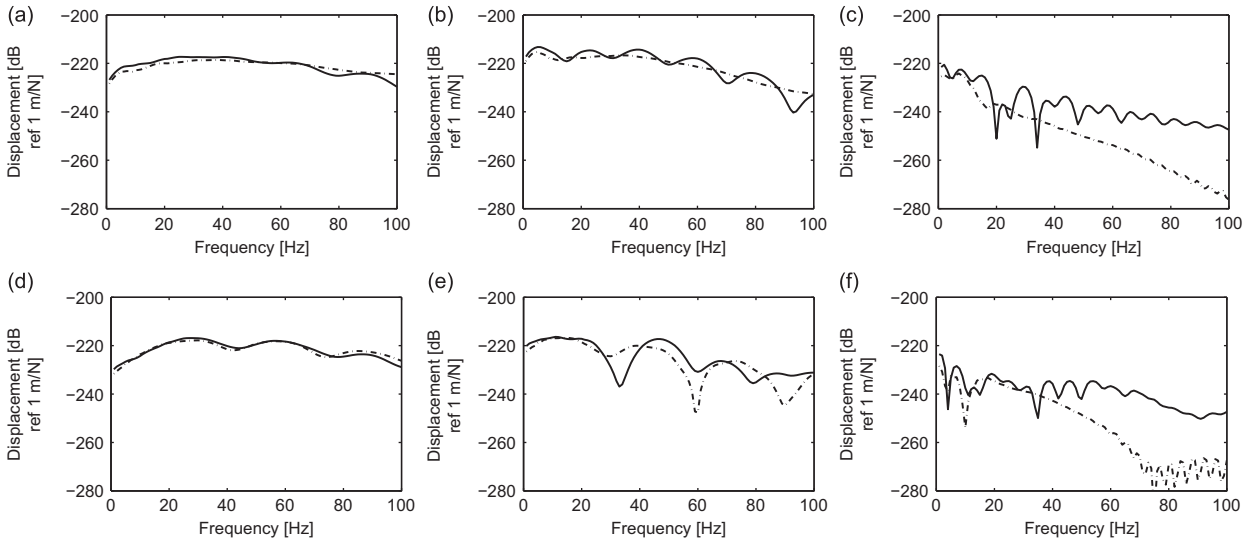

Fig. 16. Horizontal transfer function in the free field at (a) B, (b) C, (c) D, (d) F, (e) G and (f) H for a tunnel embedded in a dry (solid line) and a saturated (dash-dotted line) half-space.

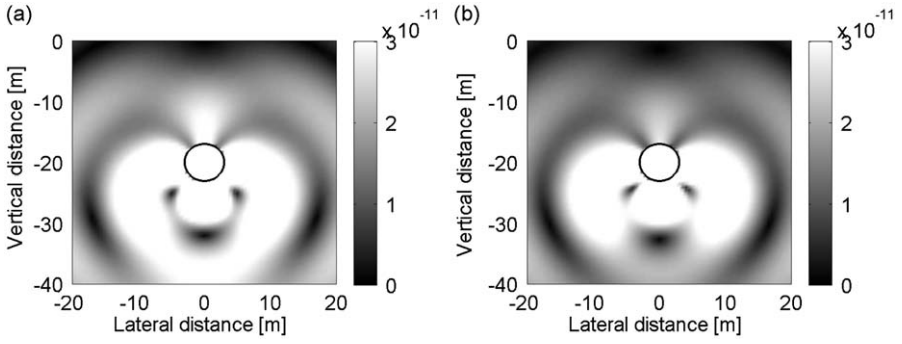

Fig. 17. The norm of the free field displacement vector at a harmonic excitation of 10 Hz for a tunnel embedded in (a) a dry and (b) a saturated full space.

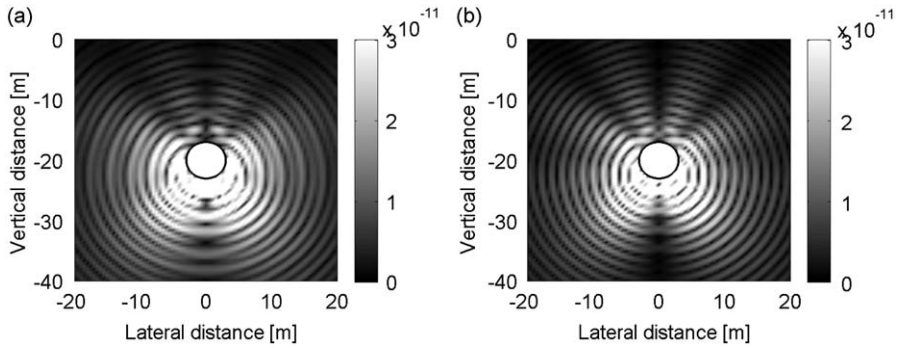

Fig. 18. The norm of the free field displacement vector at a harmonic excitation of 80 Hz for a tunnel embedded in (a) a dry and (b) a saturated full space.

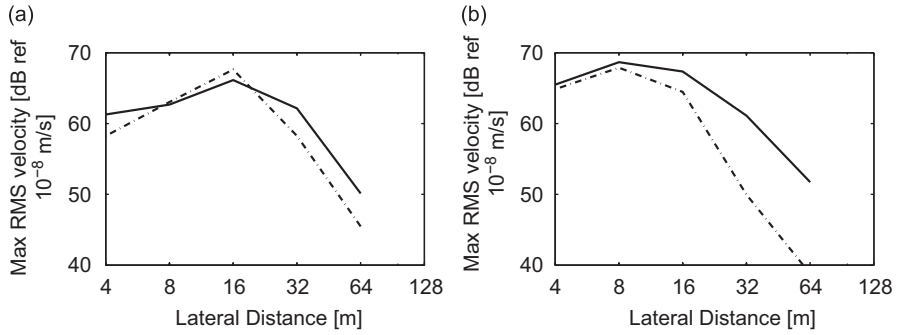

Fig. 19. Maximum RMS of (a) the vertical and (b) the horizontal velocity on the free surface as a function of the lateral distance due to a train running in a tunnel embedded in a dry (solid line) and a saturated (dash-dotted line) half-space.

5. Variation of the tunnel parameters

The tunnel properties mainly influence the wave propagation in the frequency range where the wavelengths are smaller than the size of the tunnel. The influence of the depth of the tunnel as well as the geometrical properties such as the wall thickness, size and shape of the tunnel is investigated. The change in the tunnel properties alters the energy radiation into the soil and, therefore, has a similar influence on the vertical and the horizontal component of the free field vibrations. For the sake of the brevity, only vertical components are shown in the present analysis.

5.1. Tunnel depth

Three depths of the tunnel are considered: $d_t = 10, 20$ and 30 m. The effect of the tunnel depth can be studied using the transfer functions only, as its influence on the axle loads is insignificant. Fig. 20 shows the vertical transfer function on the free surface at a varying horizontal distance from the tunnel for different tunnel depths. The general trend is that the vibration levels on the free surface decrease with tunnel depth. Thus, the vibrations from a shallow tunnel are more perceptible than the vibrations from a deep tunnel.

The excitation at the tunnel generates Rayleigh waves in the half-space at low frequencies. The contribution of Rayleigh waves to the free field response depends on the depth of the source d and is confined to frequencies less than C_R/d, where C_R is the Rayleigh wave velocity. An increase in the tunnel depth decreases the frequency range where Rayleigh waves are important.

Fig. 21 shows the maximum RMS velocity during the passage of a train in a tunnel at various points in the free field. The increase in the tunnel depth is accompanied by a decrease in the vibration levels up to a distance of 32 m. However, at larger horizontal distances from the tunnel, the influence of the tunnel depth becomes less pronounced.

5.2. Effect of structural changes in the tunnel

Two possible structural changes in the tunnel are investigated: the effect of thickening the tunnel lining and the effect of adding a tunnel invert.

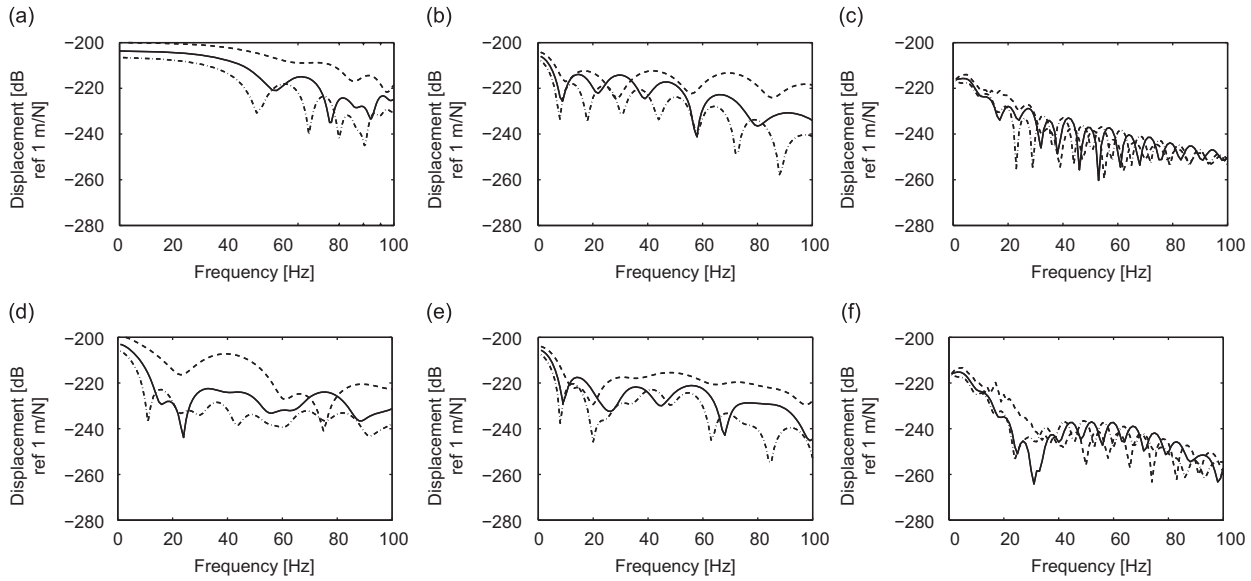

Fig. 20. Vertical transfer function in the free field at points (a) A, (b) C, (c) D, (d) E, (e) G and (f) H for a tunnel embedded at a depth $d_t = 10\,\text{m}$ (dashed line), $d_t = 20\,\text{m}$ (solid line) and $d_t = 30\,\text{m}$ (dash-dotted line) in a half-space.

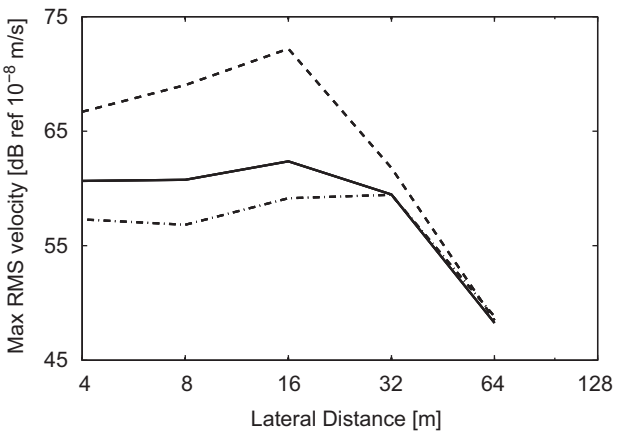

Fig. 21. Maximum RMS of the vertical velocity on the free surface as a function of the lateral distance due to a train running in a tunnel embedded at a depth $d_t = 10\,\text{m}$ (dashed line), $d_t = 20\,\text{m}$ (solid line) and $d_t = 30\,\text{m}$ (dash-dotted line) in a half-space.

These studies can be carried out by looking at the transfer functions of the coupled track–tunnel–soil system. Three wall thicknesses are considered: $t = 0.25$, 0.3 and 0.37 m. Values outside this range are not considered as they are not realistic for a tunnel with a mean radius $r_m = 2.85\,\text{m}$.

Fig. 22 shows the transfer function of the tunnel–soil system for different thicknesses of the tunnel wall. Increasing the thickness of the tunnel lining stiffens the cross section of the tunnel and increases the eigenfrequencies of the in-plane flexural modes of the free tunnel as well as increases its bending stiffness in the longitudinal direction. The variation in the thickness has a small influence on the transfer functions. This suggests that stiffening of the tunnel by increasing the thickness of the tunnel is not an efficient measure for reducing ground-borne vibrations.

Alternatively, the effect of adding material at the bottom of the tunnel is considered as a possible measure for countering ground-borne vibrations. This can be investigated by comparing the response of a tunnel with and without an invert. The effect of adding a tunnel invert is to stiffen the tunnel cross section. The concrete invert has a mass of about 368 kg/m. The tunnel with an invert is modeled using the coupled periodic finite element-boundary element model and results are compared to the reference case, where only the tunnel wall is considered. The first three in-plane flexible modes in case of a tunnel with the invert are displayed in Fig. 23, while for the case of a tunnel without the invert, the modes are displayed in Fig. 2. The eigenfrequencies of the first three in-plane modes without the tunnel invert are 17.84, 51 and 99.28 Hz. These eigenfrequencies increase to 20.98, 60.14 and 114.6 Hz when the tunnel invert is introduced in the model.

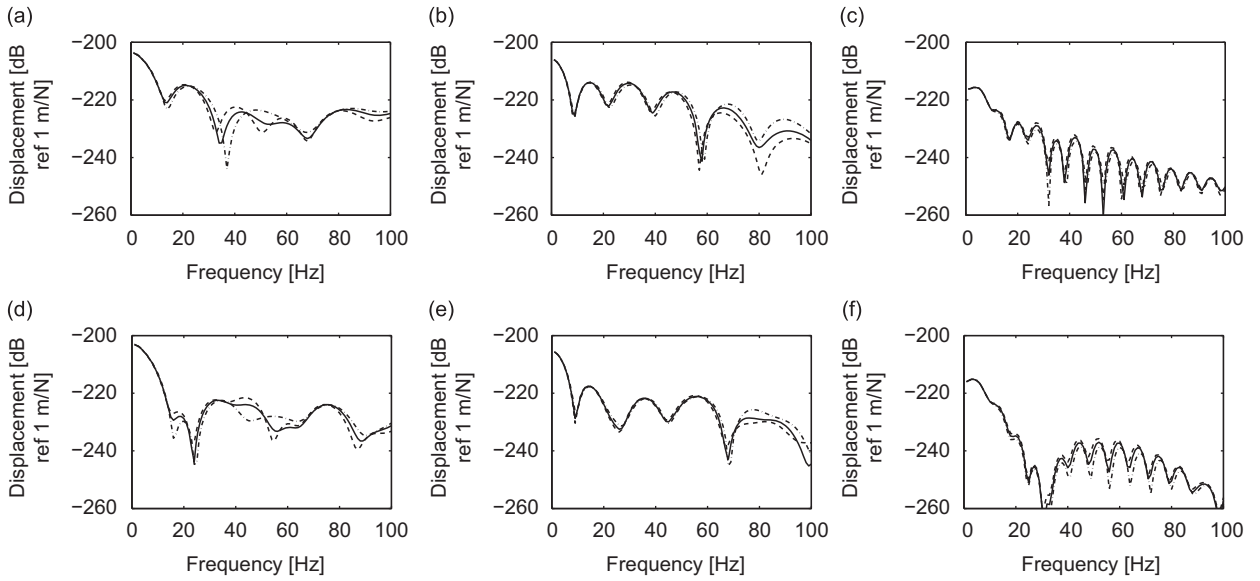

Fig. 22. Vertical transfer function in the free field at points (a) A, (b) C, (c) D, (d) E, (e) G and (f) H for a tunnel with a wall thickness $t = 0.25$ m (dashed line), $t = 0.3$ m (solid line) and $t = 0.37$ m (dash-dotted line) embedded in a half-space.

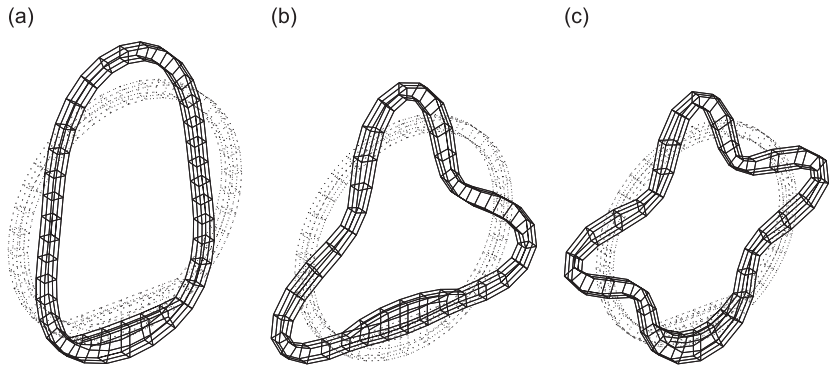

Fig. 23. The in-plane flexible modes at (a) 20.09 Hz, (b) 60.14 Hz and (c) 114.6 Hz of the reference cell of the tunnel with the concrete invert.

Fig. 24 shows the transfer function in the free field for both cases. At low frequencies, there is no change in the transfer function as wavelengths are much larger than the size of the invert. At higher frequencies, the vibration levels above the tunnel have reduced to some extent when the tunnel invert is incorporated in the model. Fig. 25 shows the norm of the instantaneous displacements at a harmonic excitation of 80 Hz for a tunnel without and with the invert, embedded in a full space. The wave propagation pattern in the vicinity of the tunnel can be observed for both cases. The tunnel invert attracts a large portion of the vibration energy, which propagates downwards. This allows the energy to radiate away from the surface, thereby causing reduction in the vibration levels in the free field above the tunnel.

This suggests that additional mass should preferably be added to the invert rather than increasing the thickness of the tunnel lining. Similar observations were also made by Unterberger et al. [36], who studied the influence of lining thickness and grout body under the tunnel invert.

5.3. Tunnel size

In the following, the influence of the size of the tunnel on the free field vibrations is studied. The size of the tunnel is not expected to significantly influence the track displacements and the axle loads. However, it modifies the propagation of the waves in the soil. Thus, the effect of the size of the tunnel can be studied using the transfer functions of the track–tunnel–soil system alone. Three different sizes of the tunnel are considered. The first tunnel has an external radius $r_e = 2.35$ m and a wall thickness $t = 0.3$ m. These are the dimensions of the tunnel on the Jubilee line in London. The second case is that of a medium sized tunnel with an external radius $r_e = 3$ m and a wall thickness $t = 0.3$ m [21]. These values correspond to the dimensions of the tunnel north of Chengfulu station on metro line 4 in Beijing. The third case is a tunnel

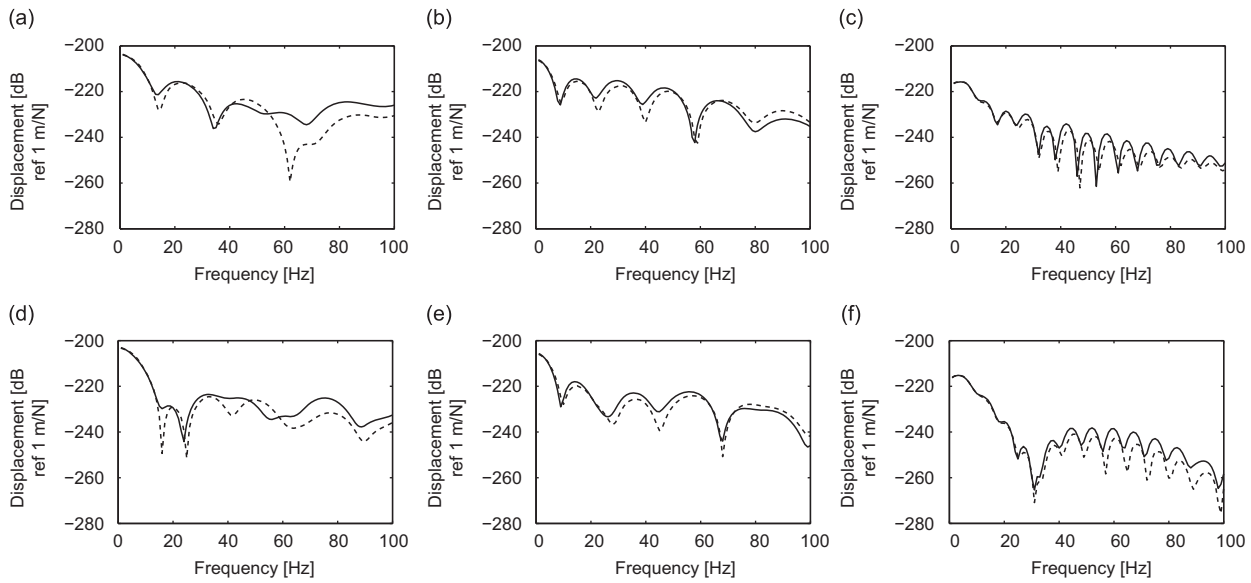

Fig. 24. Vertical transfer function in the free field at points (a) A, (b) C, (c) D, (d) E, (e) G and (f) H for a tunnel with (dashed line) and without (solid line) an invert, embedded in a half-space.

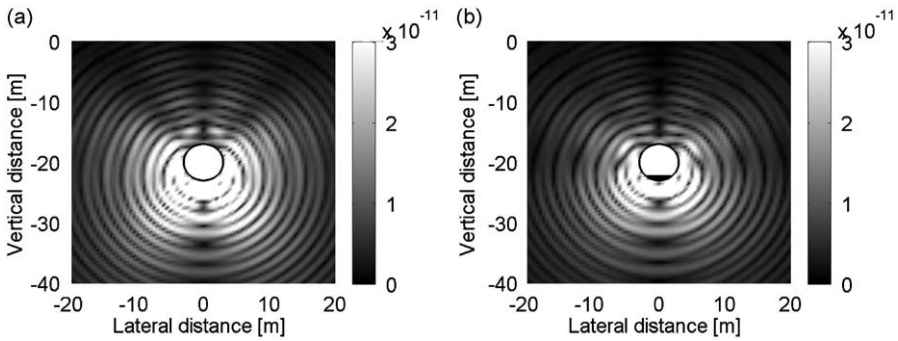

Fig. 25. The norm of the free field displacement vector at a harmonic excitation of 80 Hz for a tunnel (a) without and (b) with an invert, embedded in a full space.

with a larger radius $r_e = 4.675$ m and wall thickness $t = 0.35$ m [37]. These dimensions correspond to those of the new high speed tunnel in Antwerp. It should be mentioned that larger tunnels are usually preferred to accommodate two tracks, which results in an eccentric loading on the tunnel invert. In the present analysis, however, a larger tunnel hosting a single track is considered, and the load is applied symmetrically. The center of all tunnels is at a depth of 20 m.

The bending stiffness of the tunnel in the longitudinal direction increases with the size of the tunnel. The eigenfrequencies of the in-plane flexible modes of the tunnel decrease with the size of the tunnel, as the cross section becomes less stiff. The cut-on frequencies for the propagation of these modes into the soil in the longitudinal direction also decrease with the size of the tunnel. However, none of these modes are expected to freely propagate along the tunnel in the coupled tunnel–soil system. Thus, their effect is localized in a plane.

Fig. 26 compares the vertical transfer function in the free field for the three sizes of the tunnel. The influence of varying the size of the tunnel is quite complex and different behavior can be observed at different frequencies. The size of the tunnel has a main influence on the wave propagation in the radial direction perpendicular to the tunnel. The transfer functions are similar for the three cases at low frequencies (quasi-static response), but become different at higher frequencies due to the contribution of the various tunnel modes. At low frequencies, the wavelength(s) in the soil are much larger than the size of the tunnel and the response is not significantly affected by the presence of the tunnel. At large distances from the tunnel, the variation in the response due to the change in the tunnel size is small.

Figs. 27 and 28 show the norm of the particle displacement at a harmonic excitation of 10 and 80 Hz for different sizes of the tunnel. The frequency at which the dynamic tunnel–soil interaction becomes important decreases with the size of the tunnel. It can be observed from Figs. 27 and 28 that more energy is radiated downwards in case of the larger tunnel. This should result in a lower response on the free surface.

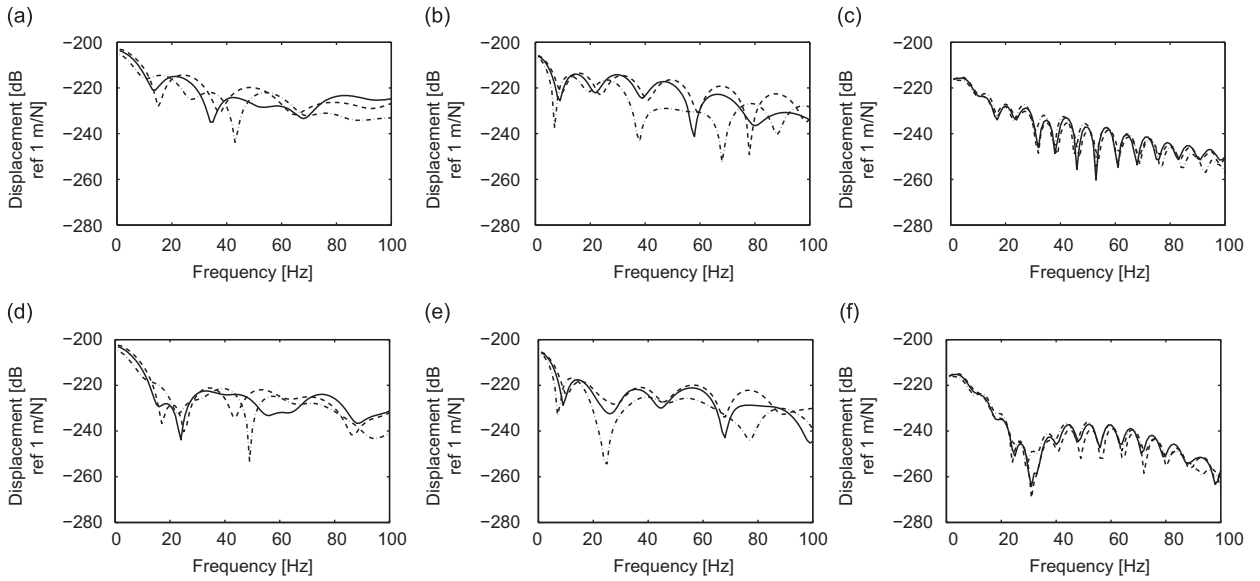

Fig. 26. Vertical transfer function in the free field at points (a) A, (b) C, (c) D, (d) E, (e) G and (f) H for a small tunnel (dashed line), a medium sized tunnel (solid line) and a large tunnel (dash-dotted line) embedded in a half-space.

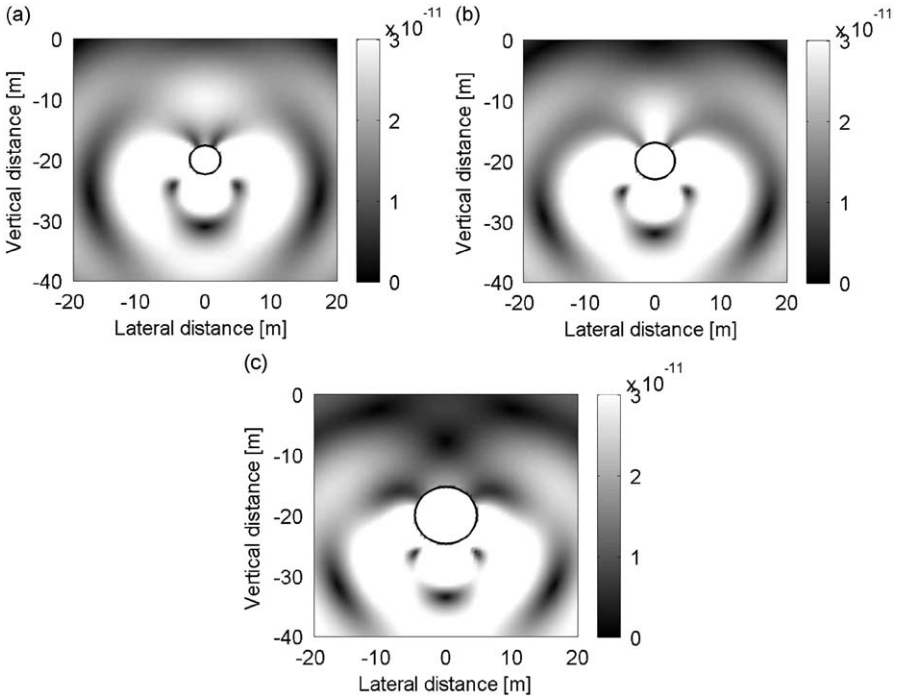

Fig. 27. The norm of the free field displacement vector at a harmonic excitation of 10 Hz for (a) a small tunnel, (b) a medium sized tunnel and (c) a large tunnel embedded in a full space.

5.4. Tunnel shape

The shape of the tunnel varies depending on the construction method. Some common cross sections of the tunnel are ovoid, horseshoe, circular or rectangular. Use of a tunnel boring machine results in a circular shaped tunnel, while the New Austrian Tunneling Method usually provides an ovoid shaped tunnel. In order to study the effect of the tunnel shape on the ground-borne vibrations, three tunnels have been considered: a tunnel with a circular cross section, a tunnel with an ovoid cross section and a tunnel with a square cross section. The geometrical properties of the second tunnel are identical to one

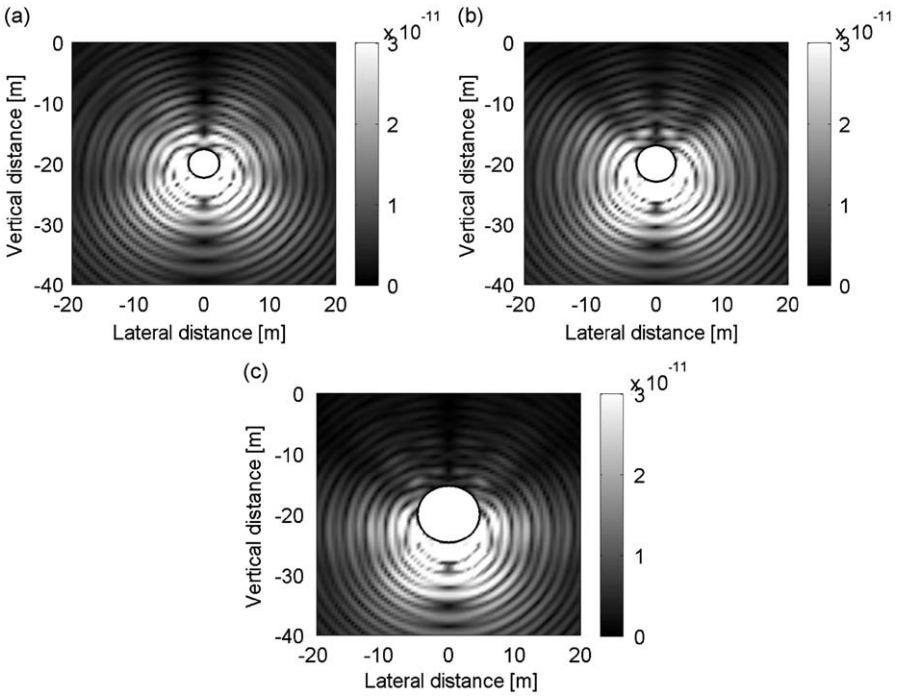

Fig. 28. The norm of the free field displacement vector at a harmonic excitation of 80 Hz for (a) a small tunnel, (b) a medium sized tunnel and (c) a large tunnel embedded in a full space.

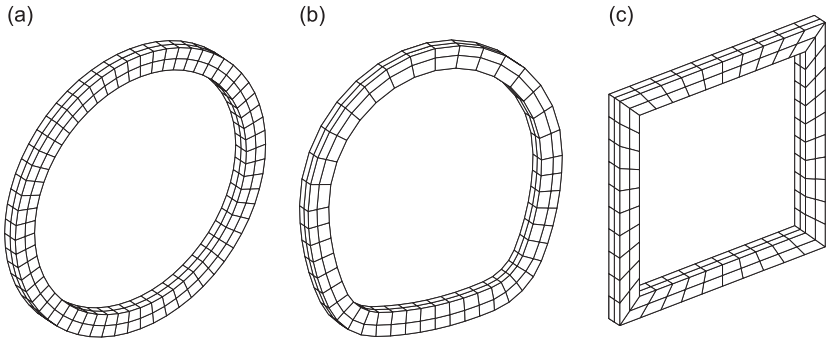

Fig. 29. Finite element mesh of the reference cell of a tunnel with (a) a circular cross section, (b) an ovoid cross section and (c) a square cross section.

of the considered (but not constructed) designs for the tunnel south of Chengfulu station on metro line 4 of Beijing. The dimensions of the ovoid cross section are 8.6 m by 8.9 m. The tunnel consists of primary and secondary linings of thickness 0.30 and 0.40 m, respectively. This results in a total wall thickness of $t = 0.70$ m. To compare with the ovoid-shaped tunnel, a circular tunnel of a larger radius is considered instead of the reference case. The circular tunnel has an external radius $r_e = 4.56$ m and a wall thickness $t = 0.70$ m. The square tunnel considered in this section has outer sides equal to 7.3 m and a wall thickness $t = 0.70$ m. The bottom of all tunnels is at 24 m. Fig. 29 shows the finite element mesh of the reference cell of the three tunnels. The moment of inertia of the circular tunnel is 165.25 m^4, while that of the tunnel with ovoid cross section and square cross section is 166.2 and 136.41 m^4. Fig. 30 shows the first in-plane flexible mode of the three tunnels. The in-plane flexural stiffness of the circular cross section and the ovoid cross section is quite similar. The square section has a lower stiffness and thus more number of modes will contribute to the response below 100 Hz.

Fig. 31 shows the vertical transfer functions on the free surface and at depth at varying distance from the tunnel. The transfer functions of the circular and ovoid tunnel are identical as the shape of these two tunnels is quite similar. The response in case of the square tunnel is different particular at points close to the tunnel and in the high frequency range. At low frequencies, the wavelengths are larger than the size of the tunnel and the shape of the tunnel does not influence the response. In the far field, the geometry of the tunnel becomes less important and the response in all three cases converges

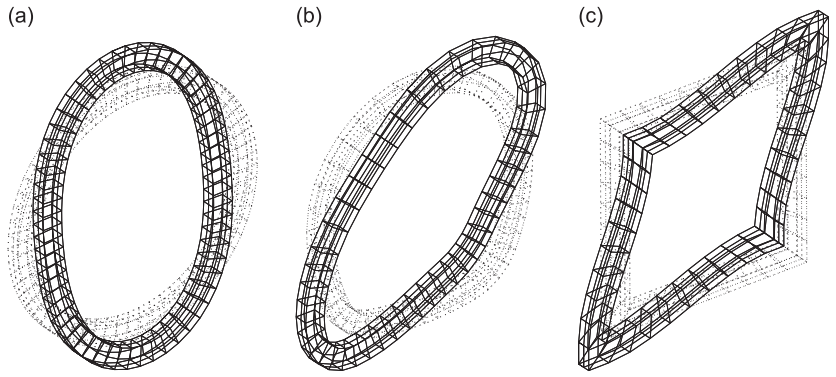

Fig. 30. The in-plane flexible mode of the reference cell of (a) the circular tunnel at 18.82 Hz, (b) the ovoid tunnel at 18.94 Hz and (c) the square tunnel at 16.80 Hz.

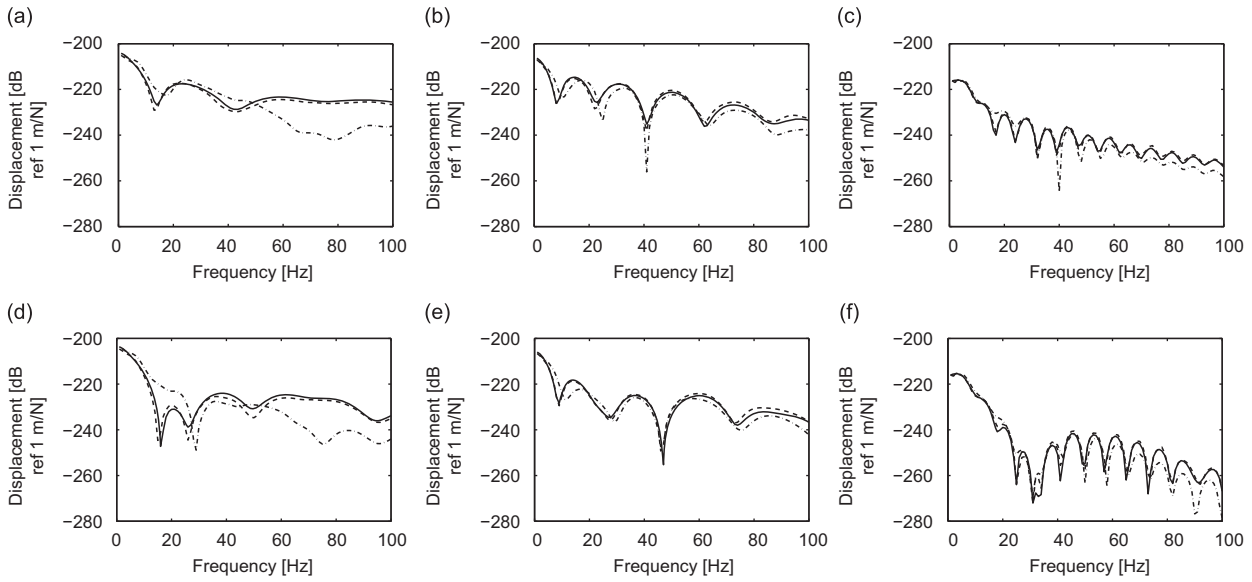

Fig. 31. Vertical transfer function in the free field at points (a) A, (b) C, (c) D, (d) E, (e) G and (f) H for the circular tunnel (solid line), the ovoid tunnel (dashed line) and the square tunnel (dash-dotted line) embedded in a half-space.

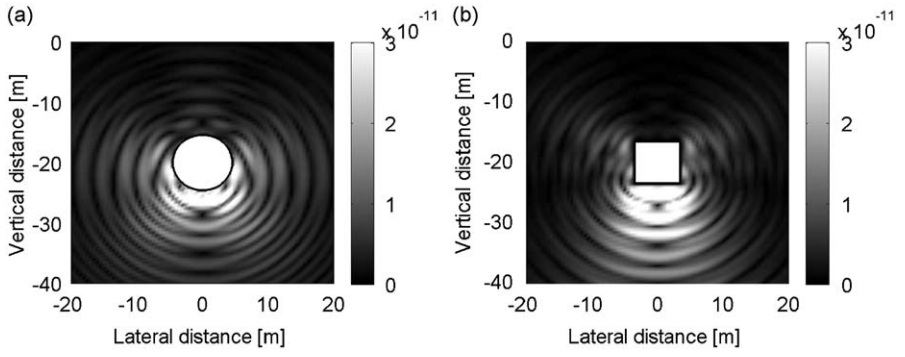

Fig. 32. The norm of the free field displacement vector at a harmonic excitation of 80 Hz for (a) a circular tunnel and (b) a square tunnel embedded in a full space.

to similar values. The lower response directly above the tunnel in case of a square cross section is due to the flat base of the section, which allows the energy to propagate downwards. This can be visualized in Fig. 32 that shows the harmonic response of the circular and square tunnel at 80 Hz.

This example demonstrates that, in order to predict the response at large distances from the tunnel, an equivalent circular cross section can be considered and simpler models such as the pipe-in-pipe model can be used to solve the problem. For accurate prediction of the response closer to the tunnel, the geometry of the tunnel has to be accounted for.

6. Conclusion

In this paper, a parametric study on the determining factors for subway induced vibrations is performed. Parameters related to the soil and the tunnel are considered and their influence on the free field response is studied. To investigate the soil and the tunnel parameters the study can be carried out by analyzing the transfer functions alone. Nevertheless, the maximum RMS velocity due to a moving train has also been computed to quantify the dependence of the free field vibrations on soil parameters. Specific conclusions that can be drawn from this study are as follows:

- The parametric study on the shear modulus has revealed that the vibration levels are higher when the tunnel is embedded in a softer soil. This is due to a decrease in the dynamic stiffness of the tunnel–soil system. At large distances from the tunnel, the vertical vibration levels in the softer and stiffer soil become comparable. This is due to larger attenuation of the waves in the softer soil. A difference of about 4–6 dB in the maximum RMS of the vertical velocity on the free surface above the tunnel is observed due to a 50 percent variation in the shear modulus. The influence of a change in the shear modulus on the horizontal vibrations is limited.
- The material damping ratio of the soil has a strong influence on the vibrations in the high frequency range and at large distances from the tunnel. A difference of more than 5 dB in the maximum RMS velocity is observed due to a 50 percent variation in the material damping ratio.
- The vibration levels in the saturated soil are less than in the dry soil due to the incompressibility of the medium. The saturation of the medium has a bigger influence on the horizontal vibrations than on the vertical vibrations.
- The vibration levels on the free surface decrease with the tunnel depth. The depth of the tunnel has a maximum effect on the free field response above the tunnel. At larger horizontal distances, the influence of the tunnel depth is less significant. This is due to the fact that for points farther away from the tunnel, the distance between the source and the receiver varies slowly with tunnel depth.
- The effect of the structural changes in the tunnel such as thickening of the tunnel lining and adding a mass at the bottom of the tunnel can be observed at higher frequencies, where the wavelengths in the soil are less than the size of the tunnel. Thickening the tunnel lining has a small influence on the vibration levels in the free field, while adding mass at the bottom of the tunnel has a greater influence and causes reduction in the vibration levels above the tunnel.
- The influence of the geometric properties of the tunnel is maximum in the vicinity of the tunnel. It has been observed that a larger tunnel results in a smaller response above the tunnel as more energy is radiated downwards. Comparison of the transfer functions of the circular and ovoid tunnel embedded in a half-space shows that both tunnels behave in a similar manner. In case of a square tunnel, a lower response is obtained above the tunnel, which is due to the flat base of the tunnel.

Acknowledgments

The results presented in this paper have been obtained within the frame of the SBO Project IWT 03175 “Structural damage due to dynamic excitation: a multi-disciplinary approach”, funded by IWT Vlaanderen. This financial support is gratefully acknowledged.

The authors are grateful to Dr. Hugh Hunt and Dr. Mohammed Hussein for providing the pipe-in-pipe model that has been used to compute some results presented in this paper.

References

[1] International Organization for Standardization, ISO 14837-1:2005 Mechanical vibration—ground-borne noise and vibration arising from rail systems—part 1: general guidance, 2005.
[2] L. Andersen, S.R.K. Nielson, Reduction of ground vibration by means of barriers or soil improvement along a railway track, *Soil Dynamic and Earthquake Engineering* 25 (2005) 701–716.
[3] M. Mohammadi, D.L. Karabalis, Dynamic 3D soil-railway track interaction by BEM–FEM, *Earthquake Engineering and Structural Dynamics* 24 (1995) 1177–1193.
[4] A.A. Stamos, D.E. Beskos, 3-D dynamic analysis of large 3-D underground structures by the BEM, *Earthquake Engineering and Structural Dynamics* 24 (6) (1995) 917–934.
[5] J.A. Forrest, H.E.M. Hunt, A three-dimensional tunnel model for calculation of train-induced ground vibration, *Journal of Sound and Vibration* 294 (2006) 678–705.
[6] J.A. Forrest, H.E.M. Hunt, Ground vibration generated by trains in underground tunnels, *Journal of Sound and Vibration* 294 (2006) 706–736.
[7] M.F.M. Hussein, H. Hunt, A numerical model for calculating vibration from a railway tunnel embedded in a full-space, *Journal of Sound and Vibration* 305 (2007) 401–431.
[8] K. Müller, H. Grundmann, S. Lenz, Nonlinear interaction between a moving vehicle and a plate elastically mounted on a tunnel, *Journal of Sound and Vibration* 310 (2008) 558–586.

[9] D. Clouteau, M. Arnst, T.M. Al-Hussaini, G. Degrande, Freefield vibrations due to dynamic loading on a tunnel embedded in a stratified medium, *Journal of Sound and Vibration* 283 (1–2) (2005) 173–199.
[10] G. Degrande, M. Schevenels, P. Chatterjee, W. Van de Velde, P. Hölscher, V. Hopman, A. Wang, N. Dadkah, Vibrations due to a test train at variable speeds in a deep bored tunnel embedded in London clay, *Journal of Sound and Vibration* 293 (3–5) (2006) 626–644.
[11] X. Sheng, C.J.C. Jones, D.J. Thompson, Prediction of ground vibration from trains using the wavenumber finite and boundary element methods, *Journal of Sound and Vibration* 293 (2006) 575–586.
[12] L. Andersen, C.J.C. Jones, Coupled boundary and finite element analysis of vibration from railway tunnels—a comparison of two- and three-dimensional models, *Journal of Sound and Vibration* 293 (2006) 611–625.
[13] Y.B. Yang, H.H. Hung, A 2.5D finite/infinite element approach for modeling visco-elastic bodies subjected to moving loads, *International Journal for Numerical Methods in Engineering* 51 (2001) 1317–1336.
[14] Y.B. Yang, H.H. Hung, D.W. Chang, Train-induced wave propagation in layered soils using finite/infinite element simulation, *Soil Dynamics and Earthquake Engineering* 23 (2003) 263–278.
[15] X.C. Bian, E.X. Zeng, Y.M. Chen, Ground motions generated by harmonic loads moving in subway tunnel, *Proceedings of the Third International Symposium on Environmental Vibrations*: *Prediction, Monitoring, Mitigation and Evaluation*. ISEV 2007, Taipei, Taiwan, November 2007.
[16] S. Gupta, M.F.M. Hussein, G. Degrande, H.E.M. Hunt, D. Clouteau, A comparison of two numerical models for the prediction of vibrations from underground railway traffic, *Soil Dynamics and Earthquake Engineering* 27 (7) (2007) 608–624.
[17] S. Gupta, Numerical Modelling of Subway Induced Vibrations, PhD Thesis, Department of Civil Engineering, K.U.Leuven, 2008.
[18] Y.B. Yang, H.H. Hung, Soil vibrations caused by underground moving trains, *Journal of Geotechnical and Geoenvironmental Engineering* 134 (11) (2009) 1633–1644.
[19] G. Lombaert, G. Degrande, J. Kogut, S. François, The experimental validation of a numerical model for the prediction of railway induced vibrations, *Journal of Sound and Vibration* 297 (3–5) (2006) 512–535.
[20] H. Chebli, R. Othman, D. Clouteau, Response of periodic structures due to moving loads, *Comptes Rendus Mécanique* 334 (2006) 347–352.
[21] S. Gupta, W. Liu, G. Degrande, G. Lombaert, W. Liu, Prediction of vibrations induced by underground railway traffic in Beijing, *Journal of Sound and Vibration* 310 (2008) 608–630.
[22] A. Hamid, T.L. Yang, Analytical description of track-geometry variations, *Transportation Research Record* 838 (1981) 19–26.
[23] M.F.M. Hussein, H.E.M. Hunt, Dynamic effect of slab discontinuity on underground moving trains, *Proceedings of the 11th International Congress on Sound and Vibration*, St. Petersburg, Russia, July 2004.
[24] M.F.M. Hussein, L. Rikse, S. Gupta, H.E.M. Hunt, G. Degrande, J.P. Talbot, S. François, M. Schevenels, Using the PiP model for fast calculation of vibration from a railway tunnel in a multi-layered half-space, *Ninth International Workshop on Railway Noise*, Munich, Germany, September 2007.
[25] D. Clouteau, D. Aubry, M.L. Elhabre, E. Savin, Periodic and stochastic BEM for large structures embedded in an elastic half-space, *Mathematical Aspects of Boundary Element Methods*, CRC Press, London, 1999, pp. 91–102.
[26] D. Clouteau, M.L. Elhabre, D. Aubry, Periodic BEM and FEM–BEM coupling: application to seismic behaviour of very long structures, *Computational Mechanics* 25 (2000) 567–577.
[27] M.L. Elhabre, Modélisation de l'interaction sismique sol-fluide-parois moulées suivant une approche périodique, PhD Thesis, Laboratoire de Mécanique des Sols, Structures et Matériaux, Ecole Centrale de Paris, 2000.
[28] L. Karl, Dynamic Soil Properties out of SCPT and Bender Element Tests with Emphasis on Material Damping, PhD Thesis, Universiteit Gent, 2005.
[29] S. Nazarian, M.R. Desai, Automated surface wave method: field testing, *Journal of Geotechnical Engineering, Proceedings of the ASCE* 119 (7) (1993) 1094–1111.
[30] D. Yuan, S. Nazarian, Automated surface wave method: inversion technique, *Journal of Geotechnical Engineering, Proceedings of the ASCE* 119 (7) (1993) 1112–1126.
[31] C.J.C. Jones, D.J. Thompson, M. Petyt, A model for ground vibration from railway tunnels, *Transport, Proceedings of the Institution of Civil Engineers* 153 (2) (2002) 121–129.
[32] Federal Railroad Administration, High-Speed Ground Transportation Noise and Vibration Impact Assessment: HMMH Report No. 293630-4, 2005.
[33] M.A. Biot, Theory of propagation of elastic waves in a fluid-saturated porous solid. I. Low-frequency range, *Journal of the Acoustical Society of America* 28 (2) (1956) 168–178.
[34] M.A. Biot, Theory of propagation of elastic waves in a fluid-saturated porous solid. II. High-frequency range, *Journal of the Acoustical Society of America* 28 (2) (1956) 179–191.
[35] M. Schevenels, G. Degrande, G. Lombaert, The influence of the depth of the ground water table on free field road traffic induced vibrations, *International Journal for Numerical and Analytical Methods in Geomechanics* 28 (5) (2004) 395–419.
[36] W. Unterberger, R. Poisel, C. Honeger, Numerical prediction of surface vibrations caused by high-speed rail traffic in tunnels, *Proceedings of the World Tunnel Congress*, Vienna, Austria, April 1997.
[37] L. Schillemans, Impact of sound and vibration of the North–South high-speed railway connection through the city of Antwerp Belgium, *Journal of Sound and Vibration* 267 (2003) 637–649.